IEEE Access
Multidisciplinary ⋮ Rapid Review ⋮ Open Access Journal

Received November 9, 2020, accepted December 18, 2020, date of publication December 24, 2020, date of current version January 8, 2021.

Digital Object Identifier 10.1109/ACCESS.2020.3047189

Decoupled Longitudinal and Lateral Vehicle Control Based Autonomous Lane Change System Adaptable to Driving Surroundings

JINSOO KIM[1,2], JAHNG-HYON PARK[2], AND KYUNG-YOUNG JHANG[1]
[1]Department of Mechanical Convergence Engineering, Graduate School, Hanyang University, Seoul 133-791, South Korea
[2]Department of Automotive Engineering, Hanyang University, Seoul 133-791, South Korea

Corresponding author: Jahng-Hyon Park (jpark@hanyang.ac.kr)

This work was supported by the Technology Innovation Program under Grant 10076338 of the Ministry of Trade, Industry, and Energy (MOTIE), South Korea.

ABSTRACT The purpose of this study is to develop an autonomous lane change control system that adapts to variable surrounding conditions, to ensure vehicle safety and traffic flow stability. In this paper, we propose decision-making and control procedures for realizing autonomous lane changing; to this end, we consider not only behaviors for changing lanes but also those involved in approaching the lane changing state, with a focus on the controller design. A decoupled control structure and longitudinal trajectory-free control approach are suggested. We design a novel inter-vehicle spacing policy and a 3DOF lateral error vehicle dynamics model. To verify the effectiveness of our system, simulation experiments are performed for 12 scenarios, and system assessments are conducted based on four evaluation perspectives. The results confirm that our system can safely control the vehicle amidst various surrounding vehicle conditions and can also ensure vehicle motion stability. Furthermore, we solve the existing dynamic instability problem of lateral control, which arises through longitudinal acceleration variability. Another significant advantage of this model is that the controlled vehicle does not interfere with the target-lane traffic flow and smoothly synchronizes with the flow during lane changing.

INDEX TERMS Lane changing, intelligent vehicle, vehicle dynamics, control, traffic flow.

I. INTRODUCTION

According to the National Highway Transportation Safety Administration, approximately 90% of traffic accidents are caused by human error; among these, more than 10% of severe accidents occur during lane changing [1], [2]. Lane changing is one of the most conventional yet riskiest maneuvers that drivers perform on a highway. In particular, in complex traffic flows, drivers must obtain a large quantity of environmental information, including the velocities and distances relative to surrounding vehicles and the facilities-related traffic environment information. Immediate and proper decision-making and maneuvering are also required for safe lane changing [3], [4]. Thus, the driving difficulty varies according to the conditions, and expertise and increased concentration are required. To reduce human errors and labor, many advanced driver assist systems (ADASs) have been developed to commercialization stages, and Level 3 autonomous driving systems are emerging [5], [6]. Nevertheless, autonomous lane changing technologies that can adapt to variable surrounding conditions remain underdeveloped.

Lane changing involves a diverse range of motions and can be perceived as challenging because it requires changes in both longitudinal and lateral velocities as well as movement in proximity to other moving vehicles [7]–[11]. It should be noted that lane changing includes multi-stage behaviors, such as transferring the vehicle from the current lane to the adjacent one (i.e., lateral motion), searching for an acceptable empty space [i.e., acceptable lane change space (ALCS)], and aligning with this space to enter the lane (i.e., longitudinal motion) [9], [10]. Furthermore, the longitudinal behavior involved in lane changing is a critical issue in traffic flow stability. It is widely known that indiscreet lane changing (e.g., sudden cut-ins) can interfere with the traffic flow and cause severe traffic accidents, traffic oscillations, shockwaves, and

The associate editor coordinating the review of this manuscript and approving it for publication was Hai Wang.

flow breakdowns under heavy traffic conditions [4]. These phenomena have been found to correspond closely to the inter-vehicle spacing distance [1], [3]. Adequate spacing provisions between nearby vehicles facilitate safe lane changes. However, because the traffic flow capacity is inversely proportional to the spacing size, methods of determining a reasonable spacing policy must be considered. Several types of spacing policy [e.g., constant time gap (CTG) or variable time gap] have been studied as solutions for adaptive cruise control (ACC) and vehicle platooning control (VPC) systems [12]–[16]. However, almost all policies use the subject-vehicle's speed or acceleration to make determinations; thus, they are deemed inadequate to determine a desirable spacing for lane changing. In particular, some lane changes require the subject-vehicle to enter an inter-vehicle space; here, both the subject-vehicle velocity and its velocity relative to the surrounding vehicles become critical factors. In this study, we design a novel spacing policy and apply it to a longitudinal control system, to enable a vehicle to reach the lane changeable state (LCS) and ensure safe distances during lane changes.

Lane changes have been extensively investigated. In transportation research, various studies have sought to identify the lane change process, the size of the acceptance gap, and the longitudinal interaction behaviors with surrounding vehicles [17]–[26]. However, severe limitations arise when applying the models directly to an autonomous driving controller, owing to a lack of feedback control laws and vehicle dynamics information. Meanwhile, in automotive control research, various driving controllers have been studied through the approach of separating the longitudinal and lateral dynamics; generally, lane changes have been tackled in lateral dynamics by neglecting variability of the longitudinal behaviors (i.e., longitudinal velocity is assumed to be constant) [27]–[33]. Because longitudinal motion variations have an adverse effect on the lateral-dynamics-based controls, numerous attempts have been made to reflect these longitudinal dynamics in lane changing procedures; this has primarily been studied to design collision avoidance [34]–[36] and overtaking [37] techniques. Furthermore, research into lane change trajectory tracking procedures that couple longitudinal and lateral dynamics has recently been conducted [38], [39]. Despite their efforts, these studies have limited applicability to randomly varying surroundings.

To implement autonomous lane changing control, it is necessary to combine the perspectives of each research field; several attempts have recently been made to this end [40]–[43]. These efforts indicate that lane changing is possible in a variety of traffic scenarios; however, these systems suffer from several limitations, including limited longitudinal trajectory control, a lack of decision-making processes, and restricted hypothesis-based scenario testing. More details are presented in the next section.

The purpose of this study is to develop an autonomous lane change control system that adapts to the variable surrounding conditions, to ensure vehicle safety and traffic flow stability. First, we propose decision-making and control procedures for autonomous lane changing; these consider behaviors for not only changing lanes but also reaching the LCS. We focus on a controller design that can reach the ALCS robustly, regardless of whether this ALCS is selected via the decision-making procedure. For improved multi-motion control and organic control with a pre-applied ACC and lane keep assist system (LKAS), we adopt a decoupled control structure and a longitudinal-trajectory-free control approach. We design a novel inter-vehicle spacing policy and apply it to sliding mode control (SMC)-based longitudinal controllers. To ensure robustness against the highly variable longitudinal movements that occur during lateral control, a three degrees-of-freedom (DOF) lateral error vehicle dynamics model is designed, and adaptive model predictive control (AMPC) [which constantly predicts new operating conditions through time-varying parameters (i.e., vehicle velocity)] is adopted. To facilitate near-future realization, this system is designed to control only the subject-vehicle that intends to change lanes, instead of employing a cooperative control function with surrounding vehicles.

The remainder of this paper is organized as follows: in Section II, the literature review is presented; in Section III, we describe the procedure and control strategies used for autonomous lane changing; in Section IV, the SMC and AMPC-based controllers are designed; in Section V, we evaluate our system for various types of surrounding condition scenarios; and in Section VI, we summarize the conclusions of the study.

II. LITERATURE REVIEW

Over the past decades, numerous studies have been conducted regarding lane changes. Most lane changing models are applicable to a variety of traffic and transportation research, including transportation planning and traffic-management policy development. Recently, lane change research has primarily focused on vehicle control. As described above, it is necessary to integrate both aspects to implement an improved autonomous lane change system. In this section, we summarize previous research into two aspect categories: behavioral and control.

A. LANE CHANGE BEHAVIOR RESEARCH

Since the 1980s, numerous transportation researchers have attempted to model lane changing behaviors, using three broad modeling categories: stimulus response, discrete choice, and psychological models [8]. Discrete choice models are well-established and operate on a three step process: lane change-necessity checking, target-lane selection, and gap acceptance decision [17]–[26]. These model are also designed to represent various types of lane changing behaviors, including mandatory lane changing, discretionary lane changing, and forced lane changing. Because these models employ a deterministic process using simple regression functions or if-then-rules, they offer fast computing speeds. To implement autonomous lane changing in complex traffic

situations, models describing the lane change process and acceptance gap size appear to be essential. However, because they do not reflect the behaviors specific to vehicle control, these models are typically only used for simulating traffic flows and analyzing their effects (e.g., congestion, shock waves, and collisions).

Researchers have focused not only on identifying the procedures but also on clarifying the motion characteristics of lane change behaviors [8]. As in-vehicle and environment sensing technologies [e.g., GPS, micro-electromechanical systems (MEMSs), Gyro, vision, radar, Lidar, etc.] have been improved, various dynamic vehicle-motion characteristics (e.g., trajectory, velocity, acceleration, heading, and yaw angle) and interactions between the subject-vehicle and surrounding ones have become monitorable [8], [9]. By analyzing these data, several researchers have attempted to formulate the factor correlations associated with lane changes (e.g., lane time durations and distances, distances and velocities relative to surrounding vehicles, sizes of acceptable spacing margins, boundary conditions, etc. [17]–[26]). From this research, numerous multi-stage motions involved in lane changing have been clearly identified. Refs. [8], [9] define lane changing as a multi-stage motion; that is, it involves not only transferring the vehicle from the current lane to the adjacent one but also searching for an ALCS and aligning with it to facilitate the change. Here, an important activity required for autonomous lane changing in various traffic situations is implementing longitudinal motion to reach the LCS.

As the factors associated with lane changing have become more diverse and complex, the lane changing behavior models have been improved by applying advanced methodologies and algorithms, including cellular automata, hidden Markov models, Gaussian mixture models, fuzzy logic, and artificial neural networks [7]–[11]. Though these models describe the interactions with the surroundings and effectively capture the aforementioned characteristics, their direct application to autonomous driving controllers seems to be severely limited by a lack of feedback control laws and vehicle dynamics information.

B. LANE CHANGE CONTROL RESEARCH

In automotive control research, various vehicle driving controls have been studied from the perspective of decoupled longitudinal and lateral dynamics [14]–[16], [27]–[32]; lane changes have primarily been dealt with using lateral controls [27]–[32]. Generally, lateral controllers are designed to first plan a control reference (e.g., lateral offset or trajectory) and then implement a steering controller to track this reference. Most vehicle controllers classify using a two-layer hierarchical architecture composed of upper-level and lower-level controllers. Then, the simplified 2DOF (i.e., lateral displacement, yaw angle) lateral vehicle dynamics or kinematic lateral vehicle models are processed by the upper-level controllers. Here, various closed-loop feedback-control theories have been employed to calculate the control inputs that minimize the tracking errors of the control references.

Initially, because lane changing depends strongly on road geometry and the stability of vehicle dynamics, the steering curvature, lane changing time duration, and distance according to the driving state (i.e., vehicle speed and acceleration) has primarily been dealt with to design the lane change trajectory models [27]. Unlike lane change behavior models, most research has aimed to shift the vehicle to an adjacent lane using only the steering control, neglecting the variability of the longitudinal behaviors (i.e., the longitudinal velocity is generally assumed to be constant) [28]–[33]. Thus, the models are guaranteed only in comparatively simple free-flow conditions that do not require any interactions with surrounding vehicles. Moreover, the longitudinal motion variations adversely affect these lateral dynamics-based controls, hence some attempts have been made to reflect longitudinal dynamics for lane changing.

As active safety vehicle systems have emerged, several lane change control systems have begun to consider longitudinal dynamics for emergency lane changing [34]–[36] and overtaking [37]. These systems are designed to prevent forward collisions by steering when the vehicle is unable to stop behind the forward vehicle or obstacle, even though ACC or pre-brake control has already been initiated. Furthermore, research into lane change trajectory tracking, which couples the longitudinal and lateral dynamics, has been conducted [38], [39]. These efforts facilitate the implementation of comparatively variable longitudinal movements with lateral control, though they are limited to specific scenarios and do not reflect the variability of the surroundings. In [38], [39], MPC, a powerful solution for multi-objective coordination systems, was applied to calculate multi-control inputs (i.e., acceleration and steering angle) simultaneously, to track the control reference. However, this single coupled controller structure required a single, combined high-DOF vehicle model and subsequently a high computational complexity. Furthermore, this structure is liable to controller switching problems, which are caused by the shutdown of the other ADAS in operation. One solution to overcome these limitations is to decouple the longitudinal and lateral controls; such systems have included systems for Highway Driving Assist (HDA) and VPC [13], [44]. These systems employ ACC for longitudinal control and LKAS for lateral control, with each motion control operating simultaneously and independently.

Recently, several attempts have been made to consider longitudinal interaction behaviors with surrounding vehicles, to develop autonomous lane change systems [40]–[43]. These systems also feature a decoupled control structure. In lane-change-trajectory-based systems [40], [41], longitudinal and lateral trajectories are generated separately and combined for control reference, and the virtual trajectories that can be safely tolerated in the acceptable space are estimated using pre-designed constraints (i.e., safety distance margins or boundary conditions with surroundings).

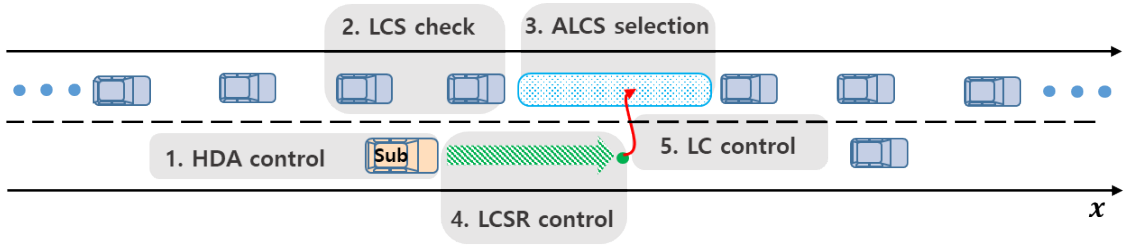

FIGURE 1. The five motion stages for autonomous lane changing.

Because they must determine an optimal trajectory in real-time, this approach cannot prevent computational overloading and tracking control error problems from arising in high- or variable-speed driving. One solution to these problems is to adopt a longitudinal-trajectory-free control approach such as ACC. In [42], [43], self-developed ACC systems were operated using lateral-based lane change controls. These efforts highlight the superiority of entirely decoupled structures and longitudinal-trajectory-free control approaches in a diverse range of traffic situations (e.g., forward-collision situations during lane changing). Even though marginally varying accel/decelerations were considered in steering motion, it remained difficult to ensure reliability in randomly varying surroundings, owing to a lack of vehicle dynamics models capable of reflecting dynamic directional forces. Furthermore, they applied a relatively simple spacing policy and neglected the decision-making process and vehicle dynamics. Moreover, the majority of aforementioned studies verify their system in fairly restricted hypothesis-based scenarios (e.g., immediate LCS scenarios), and procedures for ALCS searching or LCS reaching—important motions for lane changing—remain underresearched.

As the popularity of deep learning has increased, deep learning-based autonomous vehicle research has been conducted; most of these have focused on developing the recognition or decision processes. Several recent attempts have been made to develop vehicle control [44], [45]. These studies generated vehicle control values either through applying training maneuvers according to the driving environment (i.e., supervised learning) or through numerous trial and error virtual maneuvers in a self-designed environment (i.e., reinforced learning). Although this approach may offer advantages over the rule-based approach for recognition and decision processing, it is likely to cause inappropriate control performances because of its lack of dynamic models, the limitations of various environment designs, and long learning times. In particular, in highly variable driving scenarios (e.g., lane changing), if an abnormal action occurs even once, no matter how much data are used for training, the dynamic-model-free control can cause a very serious traffic accident. Thus, we suggest that a deep-learning-based decision and dynamic-model-based control configuration is more appropriate for implementing human-like ALCS selection and robust autonomous lane change control.

III. SYSTEM CONFIGUTATION

A. LANE CHANGING PROCEDURE

As described above, multi-stage behaviors (e.g., transferring the vehicle from the current lane to the adjacent one but also locating an acceptable empty space and aligning with it) are required for lane changing. In this respect, we categorize lane changing into a five-stage procedure (Figure 1) as follows:

Stage 1) HDA control.

If the subject-vehicle does not intend or is unable to change lanes, it maintains the current driving state and current lane using ACC and LKAS.

Stage 2) LCS check.

If a lane change is intended, the subject-vehicle determines whether lane changing is immediately possible.

Stage 3) ALCS selection.

If not in the LCS, the subject-vehicle searches for an optimal empty space that it can enter.

Stage 4) LCSR control.

After the ALCS is selected, the vehicle is instructed to reach a position from which it can enter the selected ALCS.

Stage 5) LC control.

Upon reaching the LCS, the vehicle performs steering control to change lanes.

If the subject-vehicle has already reached the LCS through Stage 2, lane changing can be conducted immediately (i.e., Stages 3 and 4 can be neglected). During Stage 5, the subject -vehicle must also conduct consecutive longitudinal controls (e.g., LCSR control) to secure a safe space that does not interfere with surrounding vehicles. After changing lanes, the subject-vehicle maintains the safe driving behavior appropriate to the new lane (i.e., return to Stage 1).

It is important to reflect such human driving behaviors in autonomous vehicle-control systems. According to psychologists, human driving is categorized into three activity levels: strategic, tactical, and control [22]. These levels are ranked in descending order of complexity, which implies that the higher the complexity, the greater the computational burden, and the less reactive the system. Generally, a human-behavior-based control system that supports automated operation must be constructed on the order of levels.

All decision-making and control procedures for autonomous lane changing are summarized in Figure 2. This system architecture is designed to replicate the hierarchical driving behaviors of humans. First, the LC intention verification step corresponds to the strategic level.

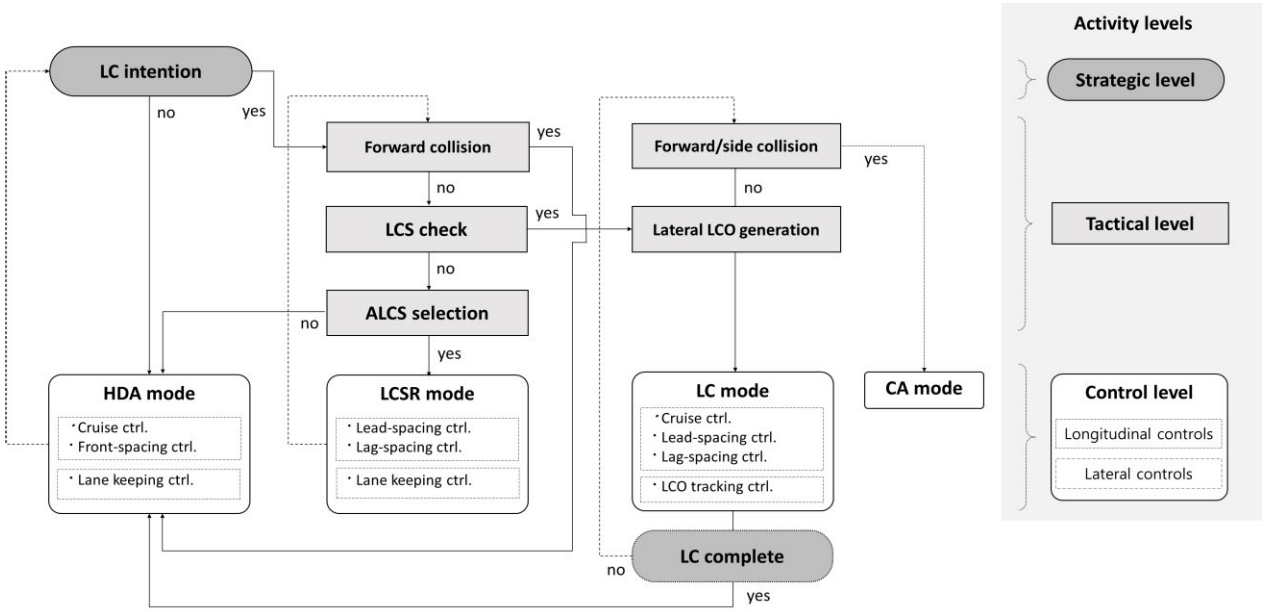

FIGURE 2. System procedures and hierarchy for autonomous lane changing.

The forward-collision check, LCS check, ALCS selection, and lane change lateral offset (LCO) generation steps correspond to the tactical level. For the control level, three types of control modes (i.e., HDA, LCSR, and LC modes) are organized to implement multi-motions in lane changing. A control mode appropriate to the surroundings and driving state is determined in real-time via the tactical level. Each of the control modes consists of decoupled longitudinal and lateral controls. To summarize, four types of longitudinal controllers (i.e., cruise controller, front-spacing controller, lag-spacing controller, and lead-spacing controller) and a single lateral-error tracking controller (i.e., for lane keeping and LCO tracking) manage all maneuvers for autonomous lane changing.

B. ASSUMPTIONS

In this paper, our research objective is to control lane changing in relatively normal traffic conditions (e.g., mandatory or discretionary lane changing), with a specific focus on the controller design. Our aforementioned system is designed to cover all motions involved in lane changes; however, it is difficult to include all the relevant aspects in one paper. Thus, we focus on vehicle control for the HDA, LCSR, and LC modes in steady state traffic flows, and we simplified the system using the following assumptions:

Assumption 1) An algorithm is required for searching and selecting an optimal ALCS from among several adjacent empty inter-vehicle spaces in the target-lane. We solve this problem by using deep learning models and training with numerous empirical lane changing data; however, this is not considered in this paper because we focus more on designing a controller that can reach the ALCS robustly. We can simply assume that an ALCS tends to be selected near the subject-vehicle in steady state traffic flow, to simplify the computing process; thus, in this study, we selected a specific empty inter-vehicle space near to the subject-vehicle as the ALCS. In addition, the controller should allow the vehicle to approach the ALCS regardless of where the space is selected because the selected ALCS can be varied according to the change of the surroundings. The lane changing performance with respect to ALCS selection is evaluated in Section V.

Assumption 2) We neglect forced lane changing. When all empty spaces in the target-lane are small (i.e., no ALCS), a cooperative control that applies a concession concept with other surrounding vehicles is required, to implement a forced lane change (e.g., cut-ins). In such cases, our system is designed to execute HDA control.

Assumption 3) The procedure for the collision avoidance (CA) mode is omitted. Our system is designed to reflect the CA control procedure, to prevent severe forward or side collisions during lane changing. This mode can be applied to our system in the future by decoupling the longitudinal and lateral dynamics and including the CA trajectory generation step. We further assume that if the distances to both the lag- and lead-vehicles are insufficient during the LC mode, the lag-vehicle tries to increase the distance to the subject-vehicle via its own spacing controls, to avoid collision.

C. CONTROL STRATEGY

1) LCS CHECKING AND ALCS SELECTION

As shown in Figure 2, when an intention to change lanes is registered, the subject-vehicle verifies forward safety and determines whether the current state is an LCS or not. The LCS checking stage (Stage 2) determines whether a lane change to the nearest inter-vehicle space is immediately acceptable, by identifying the size of the space and its position

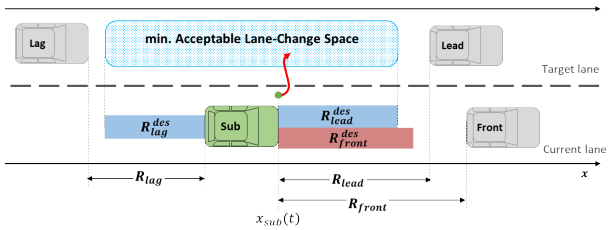

FIGURE 3. Schematic diagram of ALCS configuration and LCS.

relative to the surrounding vehicles. This stage is critical for determining whether to initiate steering control for lane changing (LC mode) or not (LCSR mode).

Figure 3 presents a schematic diagram of the LCS. The nearest inter-vehicle space exceeds the minimum size of the ALCS. The distances between the subject-vehicle and lead- and lag-vehicles are fundamental components of the desired space R^{des}, and the minimum size of the ALCS can be determined using the sum of these spaces. The formula for R^{des} is described in Section IV (A). A larger inter-vehicle space between the lead- and lag-vehicles seems to be more advantageous for changing lanes; however, the positions relative to surrounding vehicles must be considered for the LCS, to ensure safe driving and a stable traffic flow. Namely, the subject-vehicle must be ahead of the lag-vehicle's desired space and behind the lead-vehicle's one. Note that the forward desired space in the current lane must also be secured (i.e., $R_{front} \geq R^{des}_{front}$, where $R_{front} = x_{front} - x_{sub}$). The LCS condition is defined as

$$R_{lag} > R^{des}_{lag} \text{ and } R_{lead} > R^{des}_{lead} \tag{1}$$

where $R_{lead} = x_{lead} - x_{sub}$ and $R_{lag} = x_{sub} - x_{lag}$. If Condition (1) is satisfied at time t (and there is an intention to change lanes), a safe lane change is immediately possible (i.e., Stage 5). However, in the opposite case, a procedure for selecting the optimal ALCS (i.e., Stage 3) is required. Following Assumption 1, we select an empty inter-vehicle space near to the subject-vehicle as the ALCS. Through analysis of the empirical lane change data, we determined that ALCSs generally tended to be selected near the subject-vehicle during steady state traffic flow, although the current scenario is not an LCS.

When the ALCS is selected, the vehicle in front of the determined ALCS is regarded as the lead-vehicle, and the one behind it is regarded as the lag-vehicle from among the target-lane vehicles (i.e., the driving states are control references for the longitudinal controllers). If no ALCS can be selected (e.g., all inter-vehicle spaces in the target-lane are too small), the subject-vehicle executes the HDA mode (i.e., Stage 1) to maintain the current lane following Assumption 2.

2) HDA CONTROL MODE

In Stage 1 (i.e., no LC intention or no LCS or ALCS), the vehicle maintains the current driving state and lane by performing ACC and LKAS. Typically, ACC is classified into two control parts (i.e., cruise control and front-spacing control). The control conditions are

$$R_{Front} > R^{des}_{Front} \tag{2a}$$
$$R_{Front} \leq R^{des}_{Front} \tag{2b}$$

Cruise control is operated by Condition (2a), and front-spacing control is operated by Condition (2b). In the HDA mode, subject-vehicle can neglect any target-lane condition.

3) LCSR CONTROL MODE

In Stage 4 (i.e., LCS is not satisfied but ALCS is selected), the LCSR mode, which is composed of two types of longitudinal controllers (i.e., lag- and lead-spacing controllers), is performed.

Schematic diagrams of the LCSR mode are presented in Figure 4. Figure 4a shows that the subject-vehicle reaches the LCS using lag-spacing control over time α. Figure 4b also shows the lead-spacing control over time β. As shown in Figure 2, the procedures of forward-collision checking, ALCS selection, and LCSR control are conducted iteratively in real-time. At every step of the LCSR mode, one of the longitudinal controllers is selected according to the following conditions:

$$R_{Lead} > R^{des}_{Lead} \text{ and } R_{lag} \leq R^{des}_{lag} \tag{3a}$$
$$R_{Lead} \leq R^{des}_{Lead} \text{ and } R_{lag} > R^{des}_{lag} \tag{3b}$$

Lag- and lead-spacing controls are selected via Conditions (3a) and (3b), respectively. During spacing control, lateral controls are applied to maintain the current lane.

As mentioned above, the lag- and lead-vehicles are determined by the ALCS selection, and the ALCS can be varied according to the change of surroundings (i.e., the control references can vary according to the driving surroundings); this

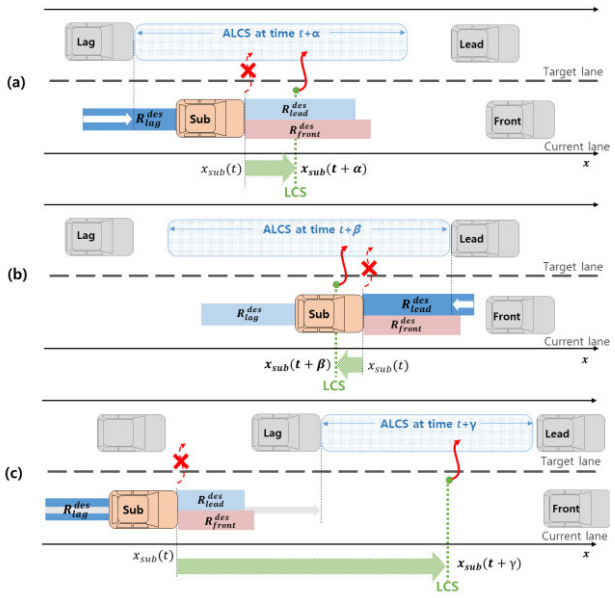

FIGURE 4. Schematic diagrams of spacing controls in LCSR mode: (a) lag-spacing control, (b) lead-spacing control, and (c) lag-spacing control when ALCS is far from subject-vehicle.

concept ensures that longitudinal control can be implemented in the approach of any ALCS, regardless of the position of the space. Figure 4c presents a schematic diagram for the case in which an ALCS is not selected in close proximity. Even in this case, the subject-vehicle should still reach the LCS during time γ, by using the lag-spacing control.

When the subject-vehicle has satisfied the LCS [i.e., it satisfies Condition (1)] via the iterative procedure, the LCSR mode is completed and the LC mode can begin. Otherwise, if no ALCS can be selected during the iterative procedure, the HDA mode is executed until a new ALCS is found. Note that the other conditions [i.e., Conditions (3a) and (3b)] have already been filtered out by the previous steps (i.e., the LCS checks or failure to select an ALCS).

4) LC CONTROL MODE

In Stage 5 [i.e., the LCS condition is satisfied at time t or the LCSR mode completed satisfying Condition (1)], safe lane changing is possible, as shown in Figure 3. To produce appropriate reactions during LC mode execution under varying surrounding conditions, steps for forward and side collision checks, LCO generation, and LC control modes are conducted iteratively in real time.

Even though the LC mode has begun (i.e., the LCS was already secure), the lag- and lead-spacing controls (which are identical to the LCSR mode) must be performed under the same conditions as the LCSR mode [i.e., Conditions (3a) and (3b)] because of the variable surrounding states. Unlike the LCSR mode, the cruise control system also maintains the flow speed of the target-lane during lane changes, using Condition (1). When the LC mode is performed after the LCSP mode, we further apply a small extra distance ed to Condition (1), to eliminate the chattering caused by control switching between the spacing and cruise controls and ensure smooth lane changing (i.e., $R_{lag} - R_{lag}^{des} > -ed$ and $R_{lead} - R_{lead}^{des} > -ed$). Moreover, even though the lag-vehicle is faster than the subject-vehicle when $R_{lag} \leq R_{lag}^{des}$ and $R_{lead} \leq R_{lead}^{des}$ during the LC mode, lead-spacing control is conducted preferentially, following Assumption 3 (i.e., we assume that the lag-vehicle will decelerate to secure the distance to the subject-vehicle and avoid collision).

Using this iterative procedure, the LCO is generated in real-time and applied to the reference of the lateral controller. After completing the LC mode via the iterations, the HDA mode control is executed to maintain speed in the new lane. If any sudden possible collision situation occurs in front or to the side of the subject-vehicle, the CA mode can be executed to avoid the collision; however, following Assumption 3, we omit this scenario here.

IV. CONTROLLER DESIGN

As shown in Figure 5, the system process can be divided into two components: a decision-making process and a control process. The decision-making process applies three steps: control mode selection, longitudinal controller selection, and lateral offset selection. First, the appropriate control mode is selected according to the surrounding conditions. Depending on the selected control mode, one of the longitudinal controllers in each mode (see Figure 2) is selected. As described in Section III, the selections are based on the relationship between R and R^{des}. Meanwhile, a lateral controller, which is based on lateral error states, is applied equally to all control modes to perform lane keeping and lane changing operations; however, the generated LCO is applied to control reference of the LKAS in the LC mode.

The control process of our autonomous lane change system is designed to decouple the longitudinal and lateral controls, enabling better multi-motion control and facilitating organic

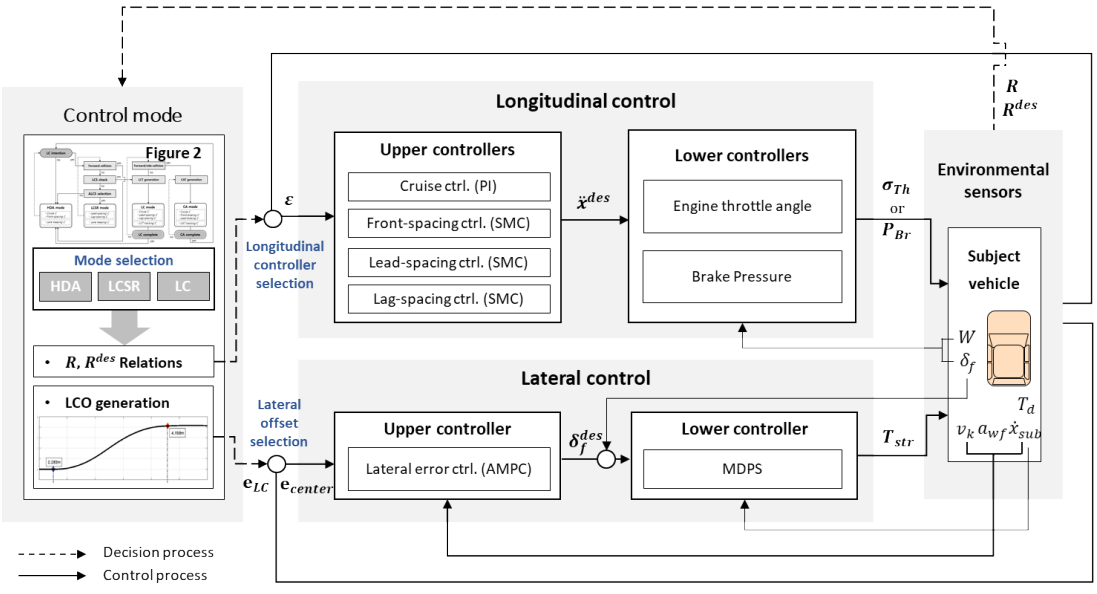

FIGURE 5. System process and decoupled longitudinal and lateral control configuration for autonomous lane changing.

control with the ACC and LKAS already in use. Each control is designed with separate upper and lower controllers. For longitudinal control, the upper level of the cruise control is designed using a simple proportional integral (PI) controller, and the spacing controllers are designed using the SMC, to reflect the desired nonlinear spacing policy (discussed in the next section). Owing to the disadvantages of longitudinal-trajectory-based control in variable surrounding conditions (e.g., computational overload and tracking control error), we adopt a longitudinal-trajectory-free control approach to determine spacing. For the lateral controller, a 3DOF lateral error vehicle dynamics model is designed, and an AMPC is adopted for its robustness against highly variable longitudinal movement (i.e., time-varying velocity). Lower controllers calculate the final control inputs of throttle angle, brake pressure, and steering torque, to implement each desired control input calculated by the upper level controllers.

A. LONGITUDINAL CONTROL

1) NONLINEAR SPACING POLICY

Establishing a spacing policy that determines a proper desired space is very important for LCS verification and spacing controls. The subject-vehicle velocity and its velocity relative to surrounding vehicles are critical parameters in determining the spacing size. We establish a nonlinear spacing policy combining the CTG policy and R-$\dot{\text{R}}$ diagram. The CTG policy can be expressed as

$$S^{des} = T_h \cdot \dot{x}_{sub} + d_{cl} \tag{4}$$

where T_h is the time headway coefficient, $\dot{x}_{sub}$ is the longitudinal velocity of the subject-vehicle, and d_{cl} is the standstill distance. Likewise, the CTG-based desired space considers only the subject-vehicle, and it does not reflect the relative velocities between the subject and surrounding vehicles. In particular, these relative velocities are critical for lane changing.

Extending the R-$\dot{\text{R}}$ diagram concept, which is widely used to determine the switching point in ACC systems, to lane changes, the relation can be expressed as

$$R^{des} = -T_\alpha \cdot \dot{R} + S_0 \tag{5}$$

where $\dot{R}$ is the relative velocity between the subject-vehicle and the surrounding ones; it is expressed as $\dot{x}_{fw} - \dot{x}_{bw}$. The *fw* and *bw* denote the forward and backward vehicles, respectively (i.e., the front- and lead-vehicles are *fw* when the subject-vehicle is *bw*, but the subject-vehicle is *fw* when the lag-vehicle is *bw*). T_α is the slope of the control switching line, and S_0 is the desirable space when $\dot{R}$ is zero. According to $\dot{x}_{bw}$, T_α and S_0 must be variables rather than constants. In this respect, $T_\alpha = \alpha \cdot \dot{x}_{bw}$. Here, α is the slope determinant coefficient, and S_0 can be replaced with S^{des}. Combining Eqs. (4) and (5), R^{des} can be derived as

$$R^{des} = \begin{cases} \left\{T_h - \alpha\left(\dot{x}_{fw} - \dot{x}_{bw}\right)\right\}\dot{x}_{bw} + d_{cl} & as\ T_h \geq \alpha\left(\dot{x}_{fw} - \dot{x}_{bw}\right) \\ d_{cl} & as\ T_h < \alpha\left(\dot{x}_{fw} - \dot{x}_{bw}\right) \end{cases} \tag{6}$$

Eq. (6) is depicted in Figure 6, and we identified that this spacing policy exhibits nonlinearity. As shown in Figure 6a, R^{des} is a quadratic function that depends on the varying slope $T_h - \alpha\left(\dot{x}_{fw} - \dot{x}_{bw}\right)$ w hen $\dot{R}$ is 0 and R^{des} is identical to S^{des} of the CTG policy concept. However, if $\dot{R}$ is larger (or smaller) than 0, R^{des} is made smaller (or larger) than S^{des} by reducing (or increasing) the slope. The dashed lines in Figure 6b also show the variation of S^{des} and T_α with respect to $\dot{x}_{bw}$. This nonlinear property of the spacing policy can explain spacing behavior in lane changing and facilitates human-like motions in autonomous driving. Following the conditions in Section III, spacing control and cruise control are conducted in the lower and upper regions of R^{des}, respectively.

2) LONGITUDINAL UPPER CONTROLLERS

Four types of longitudinal controllers are considered in this system. The cruise controller is designed based on PI control.

$$U_{CC} = \ddot{x}^{des} = k_p\left(\dot{x}_{sub}^{des} - \dot{x}_{sub}\right) + k_I \int \left(\dot{x}_{sub}^{des} - \dot{x}_{sub}\right) \tag{7}$$

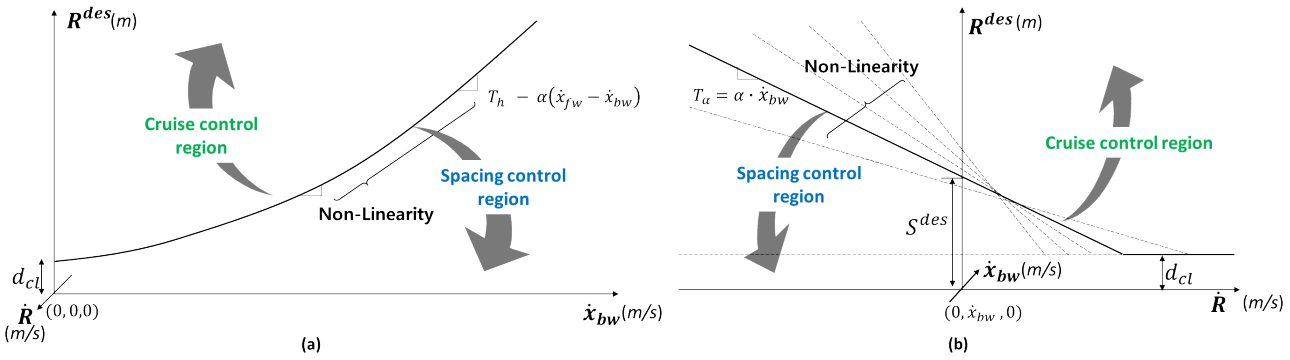

FIGURE 6. Schematic diagrams of nonlinear spacing policy for lane changing, according to perspectives of (a) desired spacing and backward vehicle velocity and (b) desired spacing and relative velocity.

where $\ddot{x}^{des}$ is the desired acceleration of the subject-vehicle and used as a control input for cruise control. k_p and k_i denote the proportional and integral gains, respectively. $\dot{x}_{sub}^{des}$ is a desired velocity. In the HDA mode, $\dot{x}_{sub}^{des}$ is set to the current driving speed, to maintain the current speed; however, in the LC mode, it is set close to the lead-vehicle speed, to harmonize with the target-lane flow.

The SMC is used for the front-, lead-, and lag-spacing controls. The sliding surface depends on the tracking error and the derivative thereof, as follows:

$$S(t) = \left(\frac{d}{dt} + \lambda\right)^{n-1} \cdot \varepsilon\,(t) \tag{8}$$

Here, n denotes the order of the uncontrolled system and is set to 2. λ denotes the convergence rate of the sliding surface. We employ a definition of compound range error $\varepsilon(t)$ that considers the vehicle acceleration:

$$\varepsilon = R - R^{des} - t_a \cdot \ddot{x}_{bw} \tag{9}$$

Here, $R = x_{fw} - x_{bw}$ is the relative distance, t_a is the positive control gain, and $\ddot{x}_{bw}$ is the acceleration of the backward vehicle. R^{des} can be rewritten as $\alpha \cdot \dot{x}_{bw}^2 + \left(T_h - \alpha \cdot V_{fw}\right)\dot{x}_{bw} + d_{cl}$ in Eq. (6). Differentiating Eq. (9), we obtain $\dot{\varepsilon} = \dot{R} - \dot{R}^{des} - t_a \cdot \dddot{x}_{bw}$, where $\dot{R}^{des} = (2\alpha \cdot \dot{x}_{bw} + T_h - \alpha \cdot \dot{x}_{fw})\ddot{x}_{bw}$ and $\dddot{x}_{sub}$ denotes the jerk of the subject-vehicle. The dynamics of the subject-vehicle can be regarded as a first-order system, as follows:

$$\tau \cdot \dddot{x}_{sub} + \ddot{x}_{sub} = \ddot{x}^{des} \tag{10}$$

Here, τ denotes the time constant. Note that *fw* is set as the front (or lead)-vehicle, and *bw* is the subject-vehicle for front (or lead)-spacing control. Meanwhile, *fw* is set as the subject-vehicle, and *bw* is the lag-vehicle in the lag-spacing control. Here, we must take into account that the controlled vehicle is the subject-vehicle. In this respect, the desired deceleration (or desired acceleration) of the lag-vehicle can be replaced by the acceleration (or deceleration) of the subject one for lag-spacing control. Namely, $\ddot{x}_{lag}$ is replaced with $-\ddot{x}_{sub}$ for lag-spacing control; hence, $\varepsilon_{lag} = R_{lag} - R_{lag}^{des} + t_a\ddot{x}_{sub}$ and $\dot{R}_{lag}^{des} = -(2\alpha \cdot \dot{x}_{lag} + T_h - \alpha \cdot \dot{x}_{sub})\ddot{x}_{sub}$.

By integrating Eqs. (8), (9), (10), and the equations above, we design three spacing controllers to determine each control command. The final control inputs of each spacing controller are derived as

$$U_{Front} = \frac{\tau}{t_a}\left(\dot{R}_{front} + \lambda\varepsilon_{front}\right) - \frac{\tau}{t_a}\dot{R}_{front}^{des} + \ddot{x}_{sub} - \eta sgn\,(S) \tag{11}$$

$$U_{Lead} = \frac{\tau}{t_a}\left(\dot{R}_{lead} + \lambda\varepsilon_{lead}\right) - \frac{\tau}{t_a}\dot{R}_{lead}^{des} + \ddot{x}_{sub} - \eta sgn\,(S) \tag{12}$$

$$U_{Lag} = -\frac{\tau}{t_a}\left(\dot{R}_{lag} + \lambda\varepsilon_{lag}\right) + \frac{\tau}{t_a}\dot{R}_{lag}^{des} + \ddot{x}_{sub} - \eta sgn\,(S) \tag{13}$$

where η is the switching gain and $sgn(S)$ denotes the signum function of the sliding surface. The stability of these controllers is ensured using Lyapunov's direct method [16]. The switching law is determined using a candidate Lyapunov function, to guarantee stability such that the system's state trajectories in the phase plane are oriented toward the origin. To reduce the chattering phenomenon caused by the discontinuous controller term, we adjust this term by applying the time-varying boundary layer approach described in [47]. As mentioned in Section III, one of these controllers is selected according to the surrounding conditions and control mode, and it calculates the desired acceleration value as a control input. The control conditions for each longitudinal controller are summarized as follows:

$$\ddot{x}^{des} = \begin{cases} U_{CC} & at \begin{array}{l}\text{condition (1) in LC mode}\\ or\text{condition (2}a\text{) in HDAmode}\end{array} \\ U_{Front} & at \text{ condition (2b) in HDAmode} \\ U_{Lead} & at \text{ condition (3a) in LCSR}or\text{LCmode} \\ U_{Lag} & at \text{ condition (3b) in LCSR}or\text{LCmode} \end{cases} \tag{14}$$

3) LONGITUDINAL LOWER CONTROLLERS

To implement the desired acceleration $\ddot{x}^{des}$, the lower controller calculates the final longitudinal control inputs as the engine throttle angle A_{th} or the brake pressure P_{br}, as shown in Figure 7. Because longitudinal controls can be performed alongside steering operations, the lateral force and inertia must be considered in the longitudinal dynamics calculations for more accurate $\ddot{x}^{des}$ implementation. As shown in Figure 8, the longitudinal dynamics for a front-wheel drive and steering vehicle are modeled as

$$m\left(\ddot{x} - \dot{y}\dot{\psi}\right) = F_{xf} - F_{yf}\delta_f - W - \frac{1}{r_{eff}}T_{br} \tag{15}$$

where m is the vehicle mass, $\dot{\psi}$ is the yaw rate, and δ_f is the front-wheel steering angle. F_{xf} denotes the front-tire forces in the rolling direction and F_{yf} is the vertical force of the front-tire; that is, $F_{xf} - F_{yf}\delta_f$ denotes the total longitudinal tire force of the front-wheel. $W = F_{roll} + F_{aero} + F_{slope}$ denotes the sum of the rolling resistance force, aerodynamic drag force, and slope resistance, respectively. r_{eff} is the effective tire radius and T_{br} denotes the braking torque.

The simple driveline dynamics are modeled using Eq. (15). In this study, we assume the longitudinal slip between the tires and road to be zero. To summarize the velocity properties, $\dot{y}$ and $\dot{x}$ are the lateral and longitudinal velocities of the subject-vehicle at its center of gravity, respectively. Furthermore, $\dot{x}$ is

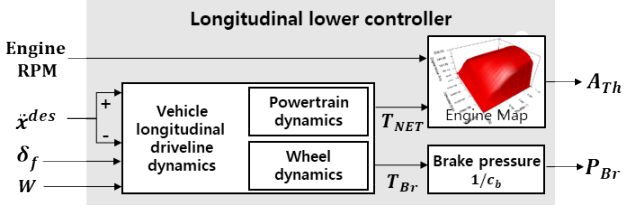

FIGURE 7. Control input calculation process in longitudinal lower controller.

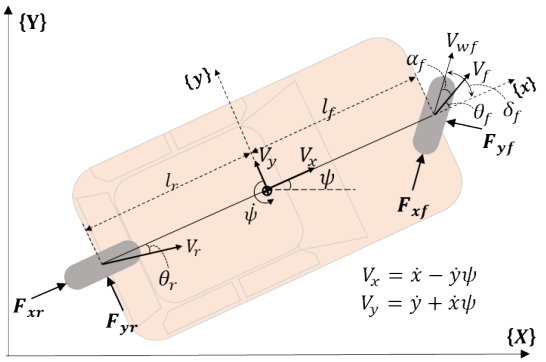

FIGURE 8. Schematic 3DOF bicycle diagram of longitudinal and lateral vehicle dynamics.

approximated as $V_{wf}\cos\delta_f$, where $V_{wf} = r_{eff}\cdot\omega_w$ denotes the front-wheel velocity. ω_w is the rotational wheel speed, which is proportional to the engine speed ω_e and relates to the gear ratio G (i.e., $\omega_w = G\cdot\omega_e$). Here, the G value is set between 1 and 0. Hence, the longitudinal acceleration is as follows:

$$\ddot{x} = r_{eff}\cdot G\cdot\dot{\omega}_e\cdot\cos\delta_f \tag{16}$$

Moreover, this model assumes that the vehicle's torque converter is locked and the transmission is in a steady state. Accordingly, the wheel's rotational dynamics are $I_w\dot{\omega}_w = T_w - r_{eff}\cdot F_{xf}$ and its transmission dynamics are $I_t\dot{\omega}_t = T_t - G\cdot T_{wheel}$, where I denotes each inertial momenta, ω_t is the transmission speed, and T_w and T_t denote the wheel and turbine torques, respectively. The engine's rotational dynamics can be defined as $I_e\dot{\omega}_e = T_{net} - T_p$, where T_p is the pump torque. Because $\omega_t = \omega_e$ and $T_t = T_p$, we have

$$\dot{\omega}_e = \frac{1}{J_e}\left\{T_{net} - Gr_{eff}W - GT_{br} - Gr_{eff}\left(F_{yf}\delta_f - m\dot{y}\dot{\psi}\right)\right\} \tag{17}$$

where $J_e = I_e + I_t + G^2I_w + mG^2r_{eff}^2\cos\delta_f$ is the effective inertia term. Because the value of $F_{yf}\delta_f - m\dot{y}\dot{\psi}$ (which denotes the difference in additional longitudinal forces between the front-wheel and center of gravity) is generally very small, this term can be neglected. Substituting Eq. (16) into Eq. (17), T_{net} and T_{br} can be derived as

$$T_{net} = \frac{J_e}{r_{eff}\cdot G\cdot cos\delta_f}\times\ddot{x}_+^{des} + Gr_{eff}W \tag{18a}$$

$$T_{br} = -\frac{J_e}{r_{eff}\cdot G^2\cdot\cos\delta_f}\times\ddot{x}_-^{des} - r_{eff}W \tag{18b}$$

where $\ddot{x}_{sub}$ is equal to $\ddot{x}^{des}$ (defined by the upper controllers). $\ddot{x}_+^{des}$ and $\ddot{x}_-^{des}$ are the positive and negative values of $\ddot{x}^{des}$, respectively. To prevent overlap, only one actuator can be operated; thus, T_{br} is neglected when $\ddot{x}^{des}\geq 0$ for T_{net}, and T_{net} is also neglected when $\ddot{x}^{des}< 0$ for T_{br}. To determine A_{th}, we use a lookup table for the engine map, which is composed of experimental data for A_{th}, T_{net}, and engine RPM. In addition, P_{br} can be approximately defined as T_{br}/c_b, where c_b is the positive gain. In this study, because the vehicle plant is substituted into the CarSim model, other parameters (including δ_f) are directly measured by the simulator in real-time. Moreover, we present only the calculation process of the lower controller and omit the detailed values of the parameters and lookup table, because the lower controller can vary as the vehicle plant changes, and we focus only on the implementation of the desired acceleration, which is determined by the upper level controllers.

B. LATERAL CONTROL

1) LATERAL ERROR DYNAMICS VEHICLE MODEL

For steering control, a 3DOF lateral error dynamics vehicle model is designed. The vehicle model, as shown in Figure 8, calculates the lateral vehicle dynamics by considering the longitudinal force. The expression for the lateral movement of the vehicle is as follows:

$$m\left(\dot{y} + \dot{x}\psi\right) = F_{yf} + F_{xf}\cdot\delta_f + F_{yr} \tag{19a}$$

$$I_z\ddot{\psi} = l_f\cdot F_{yf} + l_f\cdot F_{xf}\cdot\delta_f - l_rF_{yr} \tag{19b}$$

where F_{yf} and F_{xf} are the lateral and longitudinal tire forces of the front-wheel, respectively. F_{yr} is the lateral tire force of the rear wheel , $\dot{\psi}$ denotes the yaw rate of the vehicle, I_z denotes the yaw moment of inertia of the vehicle, and l_f and l_r are the mean longitudinal distances from the center of gravity to the front- and rear-wheels, respectively. The three tire forces can be defined as

$$F_{yf} = 2\cdot C_{\alpha f}\cdot\alpha_f \quad where\ \alpha_f = \delta_f - \theta_f \tag{20a}$$

$$F_{yr} = 2\cdot C_{\alpha r}\cdot\alpha_r \quad where\ \alpha_r = -\theta_r \tag{20b}$$

$$F_{xf} = m\cdot a_{wf} \quad where\ a_{wf} = r_{eff}\cdot\dot{\omega}_w \tag{20c}$$

where $C_{\alpha f}$ and $C_{\alpha r}$ denote the lateral cornering stiffnesses of the front- and rear-tires, respectively. α_f and α_r denote each side-slip angle of the tires. θ_f and θ_r denote the velocity angles of the tires, which are expressed as $\theta_f \simeq (\dot{y} + l_f\dot{\psi})/\dot{x}$ and $\theta_r \simeq (\dot{y} - l_r\dot{\psi})/\dot{x}$ using the small angle approximation. As mentioned above, we neglect the longitudinal slip, pitch, and roll motions of the vehicle body due to model complexity. Thus, F_{xf} can be simply estimated as $\dot{\omega}_w$, which is the rotational wheel acceleration of the front-tire. Integrating Eqs. (19) and (20), we deduce that

$$\ddot{y} = a_1\dot{y} + a_2\dot{\psi} + b_1\delta_f \tag{21a}$$

$$\ddot{\psi} = a_3\dot{y} + a_4\dot{\psi} + b_2\delta_f \tag{21b}$$

where

$$\begin{cases} a_1 = \dfrac{-2\left(C_{\alpha f}+C_{\alpha r}\right)}{m\dot{x}}, & a_2 = \dot{x}\left\{-1-\dfrac{2(C_{\alpha f}l_f - C_{\alpha r}l_r)}{m\dot{x}^2}\right\}, \\ a_3 = \dfrac{-2\left(C_{\alpha f}l_f - C_{\alpha r}l_r\right)}{I_z\dot{x}}, & a_4 = \dfrac{-2\left(C_{\alpha f}l_f^2 + C_{\alpha r}l_r^2\right)}{I_z\dot{x}}, \\ b_1 = \dfrac{2C_{\alpha f}}{m} + r_{eff}\dot{\omega}_w, & b_2 = \dfrac{l_f(2C_{\alpha f} + mr_{eff}\dot{\omega}_w)}{I_z} \end{cases} \tag{21c}$$

We expand Eq. (21) into the lateral error dynamics model by considering the road model and look-ahead distance L.

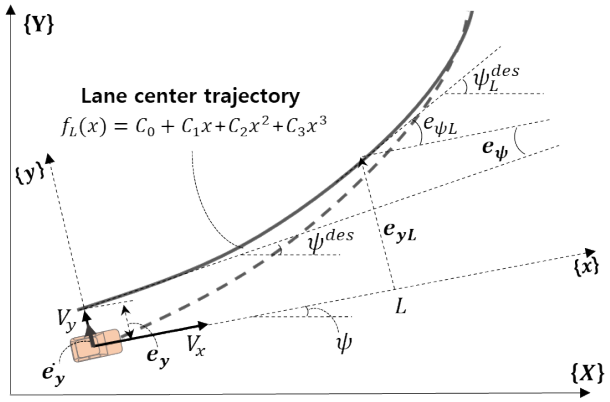

FIGURE 9. Schematic diagram of lateral error properties at the look-ahead distance point.

The lateral relationship between the road and vehicle is depicted in Figure 9. The lateral error state is set to $e_{center} = \left[e_{yL} \dot{e_y} e_\psi \dot{\psi}\right]^T$. $\dot{e_y} = V_y - V_y^{des}$ can be deduced as $\dot{y} + \dot{x}e_\psi$, where $e_\psi = \psi - \psi^{des}$. Considering the look-ahead distance, we find that $e_{yL} = y_L - y_L^{des} = e_y + Le_\psi$ and $\dot{e}_{yL} = V_{yL} - V_{yL}^{des} = \dot{e_y} + L\dot{e_\psi} + \dot{x}(e_{\psi L} - e_\psi)$. Applying these to Eq. (21), the error state space model of the lateral vehicle dynamics can be derived as

$$\dot{X} = AX + B_u U + B_v V \tag{22a}$$

$$Y = CX \tag{22b}$$

where

$$\begin{cases} X = e_{center},\ U = \delta_f,\ V = \begin{bmatrix} \dot{\psi}^{des} \\ e_{\psi L} - e_\psi \end{bmatrix}, \\ A = \begin{bmatrix} 0 & 1 & 0 & L \\ 0 & a_1 & -a_1\dot{x} & a_2 + \dot{x} \\ 0 & 0 & 0 & 1 \\ 0 & a_3 & -a_3\dot{x} & a_4 \end{bmatrix}, \\ B_u = \begin{bmatrix} 0 \\ b_1 \\ 0 \\ b_2 \end{bmatrix}, B_v = \begin{bmatrix} -L & \dot{x} \\ -\dot{x} & 0 \\ -1 & 0 \\ 0 & 0 \end{bmatrix}, \\ C = \begin{bmatrix} 1 & 0 & 0 & 0 \\ 0 & 0 & 1 & 0 \end{bmatrix} \end{cases} \tag{22c}$$

2) LATERAL OFFSET MODEL

The local coordination of the lane-center model $f_L(x)$ is defined as a third-order polynomial function of the longitudinal distance x, as shown in Figure 9. The region-of-interest images of the left- and right-hand lines are detected using a vision sensor in the longitudinal direction. Using inverse perspective projection, the polynomials of each line can be estimated [28]. Then, $f_L(x)$ is obtained by taking the average of the lines such that

$$f_L(x) = c_0 + c_1x + c_2x^2 + c_3x^3 \tag{23}$$

During driving, the coefficients $c_{0\sim4}$ are updated in real-time. Each coefficient has a different meaning and is used to estimate the lateral error states. When $x = 0$, c_0 denotes the lateral offset e_y, c_1 denotes the head angle error e_ψ, $2c_2$ is the road curvature k, and $6c_3$ is the curvature rate $\dot{k}$. Accordingly, the error states between the subject-vehicle and lane center can be defined as

$$e_{center} = \begin{bmatrix} e_{yL} \\ \dot{e_y} \\ e_\psi \\ \dot{\psi} \end{bmatrix} = \begin{bmatrix} c_0 + c_1L + c_2L^2 + c_3L^3 \\ \dot{y} + \dot{x}c_1 \\ c_1 \\ \dot{\psi} \end{bmatrix} \tag{24}$$

where $\dot{\psi}$ is directly observed from the yaw rate in the vehicle sensor, and $\dot{y}$ is estimated from the change rate of c_0 or by integrating the $\ddot{y}$ value from the MEMS sensor. By considering the curvature k, $\dot{\psi}^{des}$ can be estimated as $2c_2\dot{x}$. From the derivative of Eq. (23), the desired heading angle at the L point $e_{\psi L}$ is estimated as $\dot{f_L}(L)$. Thus, the measured disturbance vectors v_k can also be estimated as $v_k = \left[2c_2\dot{x}\ \ 2c_2L + 3c_3L^2\right]^T$.

For lane keeping control, e_{center} should converge to zero. However, additional LCOs should be considered for lane changing. In our system, the LCO is generated when the LC mode is required. Because the lane change can be performed simultaneously with the decoupled longitudinal spacing control, we extend the ramp sinusoid model [27] to consider longitudinal acceleration. The LCO is deduced as

$$y_{LC} = y_d \left[\frac{x_{LC}}{x_d} - \frac{1}{2\pi}\sin\left(\frac{2\pi x_{LC}}{x_d}\right)\right] \tag{25a}$$

where

$$\begin{cases} x_{LCT} = \dot{x}_{sub,0}t + \frac{1}{2}\ddot{x}_{sub}t^2,\ x_d = c_x \cdot V_{LC}\sqrt{\frac{y_d}{a_{yLC}}}, \\ V_{LC} = \dot{x}_{sub,0} + \ddot{x}_{sub}t, \\ a_{yLC} = (0.1 - 0.0013\dot{x}_{sub})\, g \end{cases} \tag{25b}$$

x_d denotes the total longitudinal distance traveled during a lane change, c_x is the longitudinal distance determinant coefficient, and y_d is the total lateral distance. We can set one of the lateral acceleration formulation cases a_{yLC} and adopt a normal single lane change case with relatively low lateral acceleration. g is the gravitational acceleration. By combining y_{LC} and e_{yL} of e_{center}, the new lateral error state e_{LC} (i.e., $e_{LC} = \left[e_{yL} + y_{LC}\dot{e_y}e_\psi\dot{\psi}\right]^T$) can be set, and the lateral controller generates a control input δ_f to minimize e_{LC} in the LC mode.

3) LATERAL UPPER CONTROLLER

To implement the lateral control input δ_f, the lateral upper controller that minimizes e_{center} or e_{LC} is designed by adopting an AMPC. MPC is a process control method that actively uses the dynamical system model. The system is optimized within a predefined time slot, for which the MPC estimates

the future states and controls of the system. Using Eq. (22), we discretize the model into a single-input, multi-output model using the zero-order hold method. The discrete state–space model can be expressed as

$$X_{k+1} = AX_k + B_u U_k + B_v V_k \tag{26a}$$
$$Y_k = CX_k \tag{26b}$$

where V_k is the measurement disturbance (MD). Due to rank $[B_u, AB_u \ldots An{-}1B_u] = 2n$, the pair (A, B) is controllable. The system matrices A, B_u, and B_v contain a time-varying parameter (vehicle velocity $\dot{x}$); thus, the matrices are time-varying. In this case, we can employ an AMPC that constantly predicts the new operating conditions. AMPCs can be used in linear-time-varying (LTV) systems that feature uncertainties, where the controller parameters are tuned in a closed loop employing real-time measurements. Since the model input is the control increment ΔU_k of the control signal U_k, an incremental state space model can be derived as follows:

$$\overbrace{\begin{bmatrix} X_{k+1} \\ U_k \end{bmatrix}}^{\tilde{X}_{k+1}} = \overbrace{\begin{bmatrix} A & B_u \\ 0 & I \end{bmatrix}}^{\tilde{A}} \overbrace{\begin{bmatrix} X_k \\ U_{k-1} \end{bmatrix}}^{\tilde{X}_k} + \overbrace{\begin{bmatrix} B_u \\ I \end{bmatrix}}^{\tilde{B_u}} \overbrace{(U_k - U_{k-1})}^{\Delta U_k} + \overbrace{\begin{bmatrix} B_v \\ 0 \end{bmatrix}}^{\tilde{B_v}} V_k \tag{27a}$$

$$Y_k = \overbrace{[C0]}^{\tilde{C}} \overbrace{\begin{bmatrix} X_k \\ U_{k-1} \end{bmatrix}}^{\tilde{X}_k} \tag{27b}$$

Assuming that at sampling instant k ($k > 0$), the state variable vector X_k represents the current vehicle. The future control sequence is denoted as ΔU_k, ΔU_{k+1}, ΔU_{k+2}, …, ΔU_{k+Nc-1}, where Nc is the so-called control horizon and we denote the future state variables as $\tilde{X}_{k+1}$, $\tilde{X}_{k+2}$, $\tilde{X}_{k+3}$, …, $\tilde{X}_{k+Np}$, where Np is the so-called prediction horizon. We assume that the control input is held constant beyond Nc steps (i.e., $\Delta U_{k+j}{=}\ 0$, $j = Nc, Nc{+}1, \ldots, Np - 1$). Thus, the prediction input vector ΔU_{ak}, disturbance vector V_{ak}, and output vector Y_{ak} can be defined as

$$\begin{cases} \Delta U_{ak} = \begin{bmatrix} \Delta U_k \\ \Delta U_{k+1} \\ \vdots \\ \Delta U_{k+Nc-1} \end{bmatrix}_{Nc\times 1}, V_{ak} = \begin{bmatrix} V_k \\ \vdots \\ V_{k+Nc-1} \\ \vdots \\ V_{k+Np-1} \end{bmatrix}_{Np\times 1}, \\ Y_{ak} = \begin{bmatrix} Y_{k+1} \\ \vdots \\ Y_{k+Nc} \\ \vdots \\ Y_{k+Np} \end{bmatrix}_{Np\times 1} \end{cases} \tag{28}$$

Combining Eqs. (26), (27), and (28), the predictive state variable at each future step can be deduced as

$$\tilde{X}_{ak+1} = \mathrm{f}\tilde{X}_k + \mathrm{g}\Delta U_{ak} + \mathrm{h}V_{ak} \tag{29a}$$
$$Y_{ak} = \mathrm{C}_I\tilde{X}_{ak+1} = \mathrm{F}\tilde{X}_k + \mathrm{G}\Delta U_{ak} + \mathrm{H}V_{ak} \tag{29b}$$

where

$$\begin{cases} \tilde{X}_{ak+1} = \begin{bmatrix} \tilde{X}_{k+1} \\ \tilde{X}_{k+2} \\ \tilde{X}_{k+3} \\ \vdots \\ \tilde{X}_{k+Np} \end{bmatrix}, \mathrm{f} = \begin{bmatrix} \tilde{A} \\ \tilde{A}^2 \\ \tilde{A}^3 \\ \vdots \\ \tilde{A}^{Np} \end{bmatrix}, \\ \mathrm{g} = \begin{bmatrix} \tilde{B_u} & 0 & 0 & \cdots & 0 \\ \tilde{A}\tilde{B_u} & \tilde{B_u} & 0 & \cdots & 0 \\ \tilde{A}^2\tilde{B_u} & \tilde{A}\tilde{B_u} & \tilde{B_u} & \cdots & 0 \\ \vdots & \vdots & \vdots & \ddots & \vdots \\ \tilde{A}^{Np-1}\tilde{B_u} & \tilde{A}^{Np-2}\tilde{B_u} & \tilde{A}^{Np-3}\tilde{B_u} & \cdots & \tilde{A}^{Np-Nc}\tilde{B_u} \end{bmatrix}, \\ \mathrm{h} = \begin{bmatrix} \tilde{B_v} & 0 & 0 & \cdots & 0 \\ \tilde{A}\tilde{B_v} & \tilde{B_v} & 0 & \cdots & 0 \\ \tilde{A}^2\tilde{B_v} & \tilde{A}\tilde{B_v} & \tilde{B_v} & \cdots & 0 \\ \vdots & \vdots & \vdots & \ddots & \vdots \\ \tilde{A}^{Np-1}\tilde{B_v} & \tilde{A}^{Np-2}\tilde{B_v} & \tilde{A}^{Np-3}\tilde{B_v} & \cdots & \tilde{B_v} \end{bmatrix}, \\ \mathrm{C}_I = \begin{bmatrix} \tilde{C} & 0 & 0 & \cdots & 0 \\ 0 & \tilde{C} & 0 & \cdots & 0 \\ 0 & 0 & \tilde{C} & \cdots & 0 \\ \vdots & \vdots & \vdots & \ddots & \vdots \\ 0 & 0 & 0 & \cdots & \tilde{C} \end{bmatrix}, \\ \mathrm{F} = \mathrm{C}_I\mathrm{f},\ \mathrm{G} = \mathrm{C}_I\mathrm{g},\ \mathrm{H} = \mathrm{C}_I\mathrm{h} \end{cases} \tag{29c}$$

The controller determines the sequence of control moves that minimize the sum of squared deviations of the predicted output from the lateral offset reference [i.e., Eqs. (23) and (25)], to obtain the lateral stability. In this study, the lateral vehicle dynamics were designed using the lateral-error-based state model (i.e., e_{center} and e_{LC}); hence, the cost function can be determined as

$$J_k = Y_{ak}^T Q Y_{ak} + \Delta U_{ak}{}^T R \Delta U_{ak} \tag{30}$$

where Q and R are the weight matrices of the controlled outputs and inputs, respectively. The constraints applied to the controlled variables and imposed upon the output are considered in the MPC upper controller, as follows:

$$\begin{cases} \Delta U_{min} \le \Delta U_{ak} \le \Delta U_{max} \\ U_{min} \le U_{ak} \le U_{max} \\ Y_{min} \le Y_{ak} \le Y_{max} \end{cases} \tag{31a}$$

where

$$U_{ak} = \begin{bmatrix} 1\,0\,0\cdots 0 \\ 1\,1\,0\cdots 0 \\ 1\,1\,1\cdots 0 \\ \vdots\;\vdots\;\vdots\;\ddots\;\vdots \\ 1\,1\,1\cdots 1 \end{bmatrix}_{Nc\times Nc} \times \Delta U_{ak} + \begin{bmatrix} U_{k-1} \\ U_{k-1} \\ U_{k-1} \\ \vdots \\ U_{k-1} \end{bmatrix}_{Nc\times Nc} \quad (31b)$$

$\Delta U_{min/max}$ represent the minimum and maximum angular increments of the front-wheel, $U_{min/max}$ are the minimum and maximum front-wheel angles, and $Y_{\min/max}$ are the minimum and maximum outputs, respectively.

Quadratic programming (QP) is used to solve optimization problems involving a quadratic objective function and constraints, and it is widely applied to optimize cost functions. The AMPC solves the QP problem at each time interval. The solution of the problem determines the so-called manipulated variables; these are input variables that are dynamically adjusted to keep the controlled variables at their set-points. The cost function [Eq. (30)] can be re-expressed in a standard quadratic form as

$$\min_{\Delta U_{ak}} \left(J_k = \frac{1}{2} \Delta U_{ak}{}^T \Omega \Delta U_{ak} + \Phi \Delta U_{ak} \right) \quad (32)$$

where the Hessian matrix $\Omega = 2\mathrm{G}^T Q\mathrm{G} + R$ and the column vectors $\Phi = 2(\mathrm{F}\tilde{X}_k + \mathrm{H}V_{ak})Q\mathrm{G}$. A series of optimal control inputs are computed in the control horizon by solving Eq. (32) subject to Eq. (31a). The sequence of the optimal control input vector is $\Delta U^*_{ak} = [\Delta U^*_k, \Delta U^*_{k+1}, \ldots, \Delta U^*_{k+Nc-1}]^T$. Because this is a receding horizon strategy, only the first element of ΔU^*_{ak} is used. We reject the rest and repeat the calculations at the next sampling time. The front-wheel steering angle for lane keeping or changing is determined as follows:

$$\delta_f^{des} = U_k = U_{k-1} + [\mathrm{I}, 0, \ldots, 0]\, \Delta U^*_{ak} \quad (33)$$

To estimate this, the traditional MPC controller uses the static Kalman filter (SKF). The SKF requires constant gain matrices M and depends on the plant parameters and disturbances characteristics. In AMPC, the controller uses an LTV Kalman filter (LTVKF) instead of the SKF, to generate consistent estimations with the updated plant dynamics. The off-line construction of the estimator gain M_k is replaced by a recursive on-line computation, defined through the update and prediction phases:

Update phase:

$$\begin{cases} \tilde{X}_{k|k} = \tilde{X}_{k|k-1} + M_k \left(Y_{ak-1} - \mathrm{C}_{I,k} \tilde{X}_{ak|k-1} \right) \\ M_k = (P_{k|k-1}\mathrm{C}^T_{I,k}) \left(S + \mathrm{C}_{I,k} P_{k|k-1} \mathrm{C}^T_{I,k} \right)^{-1} \\ P_{k|k} = \left(\mathrm{I} - M_k \mathrm{C}_{I,k} \right) P_{k|k-1} \end{cases} \quad (34a)$$

Prediction phase:

$$\begin{cases} \tilde{X}_{ak+1|k} = \mathrm{f}_k \tilde{X}_{k|k} + \mathrm{g}_k \Delta U_{ak} + \mathrm{h}_k V_{ak} \\ P_{k+1|k} = \mathrm{f}_k P_{k|k} \mathrm{f}^T_k + Z \end{cases} \quad (34b)$$

Here, S and Z are constant covariance matrices defined in the MPC state estimation. f_k and $\mathrm{C}_{I,k}$ are state-space parameter matrices for the entire controller state; these are defined as for the traditional MPC but with the proportions determined by the plant model updates at time k. $P_{k|k-1}$ is the state-estimation-error covariance matrix at k, constructed using the information from time $k-1$. Unlike the constant structure of the M matrix in the SKF, the LTVKF regularly updates the matrix with the updated plant dynamics. This model-updating strategy is a core issue when designing AMPC controllers. The entire controller structure is designed using the MPC Designer toolbox in MATLAB/Simulink.

4) LATERAL LOWER CONTROLLER

To implement δ_f^{des}, the lower controller determines the final lateral control inputs as the steering torque T_{str}, as shown in Figure 10. This controller is designed based on the motor-driven power steering (MDPS), which assists the driver's steering. T_{str} is obtained as

$$T_{str} = T_a + T_d - \frac{T_s}{N} + T_{\delta f} \quad (35)$$

where T_a is the assist torque, T_d is the driver torque, T_s is the self-alignment torque, and $T_{\delta f}$ is the steering control torque for autonomous lane keeping and changing. Here, we neglect T_a and T_d because the driver's maneuver does not interfere with our system (i.e., $T_d = 0$ and $T_a = 0$). N denotes the steering gear ratio of the MDPS. Based on the servo controller system, $T_{\delta f}$ can be obtained as

$$T_{\delta f} = k_{p2} \left\{ k_{p1} \left(\delta_f^{des} - \delta_f \right) - \dot{\delta}_f \right\} + k_{I1} \int \left\{ k_{p1} \left(\delta_f^{des} - \delta_f \right) - \dot{\delta}_f \right\} \quad (36)$$

where $k_{p1,2}$ and k_{I1} are the gains of the controller. T_s is also calculated as $2 \cdot \xi \cdot C_{\alpha f} \cdot \alpha_f$.

V. SYSTEM EVALUATION

A. SIMULATION AND SCENARIO SETUP

To evaluate the proposed autonomous lane change control system, a series of simulation experiments were carried out using CarSim-Matlab/Simulink co-simulations. The simulation was structured as shown in Figure 5. The simulation sampling time was set to 0.01 s. A C-Class hatchback vehicle model was used as the subject-vehicle, and the vehicle parameters were set as $m = 1300kg$, $I_z = 2873kg{\cdot}m^2$, $l_f = 1.1m$, $l_r = 1.58m$, $C_{\alpha f} = 49262N/rad$, $C_{\alpha r} = 33408N/rad$, $r_{eff} = 0.3\,m$, and $c_b = 250$. A double

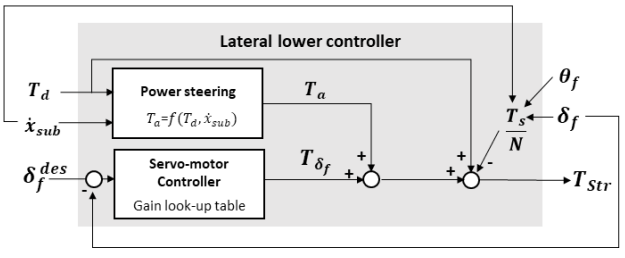

FIGURE 10. Control input calculation procedure in lateral lower controller.

TABLE 1. Controller parameters and default set value.

Longitudinal control		Lateral control	
Parameter	Value	Parameter	Value
T_h	0.5 s	c_x	2.6
d_{cl}	0.5 m	L	40 m
α	0.15	Np	10
t_a	0.2	Nc	3
τ	0.3 s	$\Delta U_{min\|max}$	±0.261 rad/s
λ	1	$U_{min\|max}$	±0.523 rad
ed	0.5 m	$Y_{min\|max}$	$\pm\begin{bmatrix} 4\text{ m} \\ 0.2\text{ rad} \end{bmatrix}$

straight lane on a zero curvature road and 3.8 m wide lanes (y_d) were set in CarSim. The default values of the parameters for the longitudinal and lateral upper controllers are listed in Table 1; these were selected to model relatively typical driving conditions. Lower controller parameter values were directly imported from the CarSim model, and the control gains were tuned by comparing the experimental and field data through trial and error.

As described in Assumption 1, we selected a reasonable empty inter-vehicle space near to the subject-vehicle as the ALCS in this study. The lead- and lag-vehicles for longitudinal control were specified according to the selected ALCS, and the scenarios were constructed according to the driving velocities and relative positions of the vehicles. In this respect, our controller is guaranteed to approach any ALCS, regardless of where it is; we validate this in the next section.

To validate the effect of our lane changing control system, we tested various scenarios; the 12 representative scenarios are summarized in Table 2. Various driving condition scenarios were set by adjusting the initial velocities and relative distances of the vehicles at the time the LC intention was registered (i.e., initial time, t = 0). Excluding Scenarios (i) and (j) (i.e., lead- or lag-vehicle deceleration), the surrounding vehicles all maintained their initial velocities through HDA control (i.e., cruise control and front-spacing control) until the simulation was completed.

TABLE 2. Simulation scenarios in terms of initial velocity and relative distances to the surrounding vehicles.

Scenario	Initial velocity (km/h)				Initial relative distance (m)		
	V_{sub}	V_{front}	V_{lead}	V_{lag}	R_{front}	R_{lead}	R_{lag}
a	70	70	70	70	30	15	-15
b	70	60	50	50	30	15	-15
c	50	60	70	70	30	15	-15
d	70	70	70	70	20	0	-25
e	70	70	70	70	30	25	0
f	70	70	80	80	20	5	-20
g^{C}	70	70	70	70	30	20	0
h^{A}	70	70	70	70	30	20	0
i^{dc}	50	60	70^{dc}	70	30	25	0
j^{dc}	50	60^{dc}	70	70	30	25	0
k^{NS}	70	80	70	70	30	40	10
$l^{dc\text{-}CS}$	50	60^{dc}	70	70	30	25	0

^{C}: Cautious driving setting / ^{A}: Aggressive driving setting
^{dc}: Deceleration
^{NS}: Non-adjacent ALCS selection / ^{CS}: ALCS selection changing

Even if the surrounding vehicles' velocities are constant, the relationships between them and the subject-vehicle (i.e., the relative distances and relative velocities) can be regarded as variable, because the driving state of the subject-vehicle changes in real-time. The scenarios can be classified into four evaluation perspectives: surrounding driving state-, driving tendency setting-, collision risk situation-, and ALCS selection-based evaluations.

B. RESULTS

Table 3 summarizes ten types of control results with respect to subject-vehicle's movement (i.e., time period and distance in LCSR and LC modes, minimum and maximum a_x and a_y, cumulative absolute acceleration $\int |a_x|$, and averaged lateral error Aver. y_e). Note that $\int |a_x|$ denotes the total longitudinal energy expended in completing the lane change. Aver. y_e is the lateral difference between the LCO and lateral vehicle position ($y_{LC} - e_y$) during lane changing control (i.e., the lateral control error). The control mode process applied during the simulation is also described.

To identify more detailed simulation results in each scenario, we present three types of time-series plots, as shown in Figures 11–13. Figure 11 shows the change in Rs (solid lines) and P^{des}s (dashed lines). Here, P^{des} indicates the marginal position of R^{des} relative to each surrounding vehicle (i.e., $P^{des} = R - R^{des}$). This figure helps to identify the relationship between the subject-vehicle position and the R^{des}s. We can also determine whether the subject-vehicle maintains a safe distance to the surrounding vehicles over time. Figure 12 shows the velocity variation of the subject and surrounding vehicles corresponding to each scenario. Longitudinal and lateral acceleration plots of the subject-vehicle are also presented in Figure 13. In this section, we evaluate the system based on the four aforementioned evaluation perspectives.

1) INITIAL SURROUNDING DRIVING STATE-BASED EVALUATION

Scenarios (a), (b), (c), (d), (e), and (f) correspond to assessments based on the initial surrounding driving state. As shown in Scenarios (a), (b), and (c) in Table 2, when the LC intention occurs, the relative distances are same, even though the vehicles are driving at different velocities in each scenario. In Scenarios (a), (d), and (e), all vehicles drive at the same velocity of 70 *km/h*, but their relative distances differ. In Scenario (f), the vehicle speed in the target-lane is 80 *km/h*, slightly higher than the subject-vehicle velocity, and the distance to the lead-vehicle is relatively short.

TABLE 3. Simulation results according to subject-vehicle movement in each scenario scenario.

Scenario	LCSR + HDA mode		LC mode		Longitudinal movement			Lateral movement			Mode$^{Controller\ process}$
	Period (s)	Dist. (m)	Period (s)	Dist. (m)	$a_x\ (m/s^2)$ Min	$a_x\ (m/s^2)$ Max	$\int \lvert a_x \rvert$	$a_y\ (m/s^2)$ Min	$a_y\ (m/s^2)$ Max	Aver.y_e (m)	
a	0.0	0.0	6.0	116.4	-0.09	0.01	0.06	-0.83	0.83	0.080	C^{CC}
b	2.6	42.5	5.6	76.8	-3.55	0.00	6.16	-0.93	1.00	0.082	B^{LE}-C^{CC}
c	2.4	41.4	5.6	108.8	0.00	3.83	5.42	-0.82	0.83	0.086	B^{LG}-C^{CC}
d	2.0	35.7	5.8	106.9	-3.04	0.48	2.66	-0.76	0.77	0.082	B^{LE}-C^{CC}
e	2.1	44.5	5.6	113.7	-0.68	3.63	4.11	-0.89	0.89	0.086	B^{LG}-C^{CC}
f	0.0	0.0	6.3	132.2	-0.00	3.07	2.29	-0.83	0.77	0.077	C^{CC}
g^C	10.4	211.2	6.0	117.0	-1.41	3.84	6.21	-0.83	0.84	0.080	$B^{LE/LG}$-$C^{LE/LG/CC}$
h^A	2.0	41.3	5.8	116.8	-0.29	3.47	2.59	-0.87	0.87	0.083	B^{LG}-C^{CC}
i^{dc}	3.8	72.0	5.8	104.6	-1.92	3.85	13.54	-0.98	0.97	0.083	B^{LG}-A^{FR}-$C^{LE/CC}$
j^{dc}	∞	∞	-0.0	0.0	-∞	∞	∞	-0.00	0.00	-	B^{LG}-A^{FR}
k^{NS}	3.2	75.1	5.2	107.3	-2.91	3.77	11.86	-1.13	0.90	0.090	$B^{LG/LE}$-$C^{CC/LG}$
$l^{dc\text{-}CS}$	5.4	99.0	5.8	106.9	-2.50	3.68	13.11	-0.76	0.77	0.079	B^{LG}-A^{FR}-B^{LE}-C^{CC}

Mode process: A = HDA mode / B = LCSR mode / C = LC mode
Controller process: CC = cruise control / FR = Front-spacing control / LE = Lead-spacing control / LG = Lag-spacing control

The simulation results show that the subject-vehicle changed lanes immediately in Scenarios (a) and (f). In Scenarios (b), (c), (d), and (e), however, it tried to reach the LCS (i.e., the LCSR mode was applied) before initiating the LC mode. Figures 11 and 13 (b–e) show that spacing controls—to ensure the desired spacing to the lead- or lag-vehicles—were conducted during both the LCSR and LC modes [i.e., lead-spacing control in Scenarios (b) and (d), and lag-spacing control in Scenarios (c) and (e)].

In Scenario (f), although the subject-vehicle was relatively near to the lead-vehicle (5 m away), immediate lane changing was possible because the velocity of the lead-vehicle was 10 *km/h* higher than that of the subject-vehicle (i.e., sufficient LCS at $t = 0$). Figure 12(f) shows that in the LC mode, cruise control was executed at the same speed in the target-lane after lane changing, and a stable traffic flow that did not interfere with the target-lane flow was ensured.

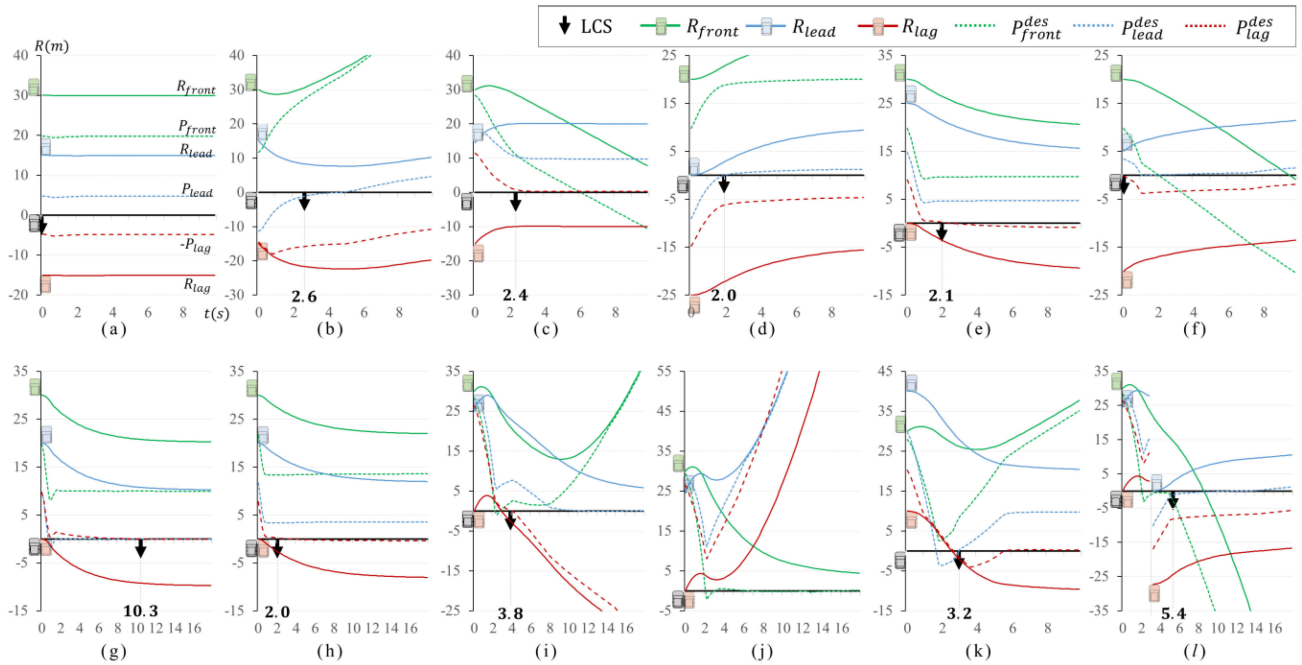

FIGURE 11. Relative distances and marginal positions of desired spaces with respect to surrounding vehicles for each scenario.

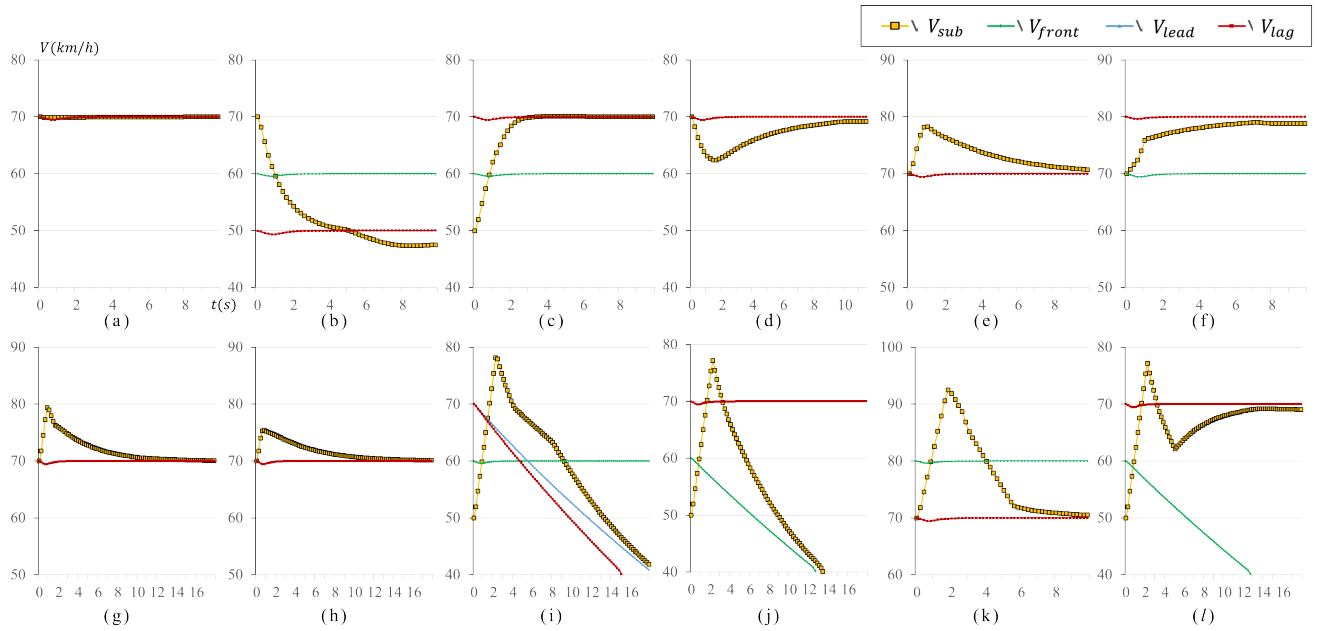

FIGURE 12. Velocity diagrams of the subject vehicle and surrounding vehicles for each scenario.

2) DRIVING TENDENCY SETTING-BASED EVALUATION

By comparing Scenarios (g) and (h), we assessed the lane changing performance with respect to the driving tendency parameter setting. In all scenarios except (g) and (h), identical parameter settings based on relatively normal driving conditions were given, as shown in Table 1; however, in Scenarios (g) and (h), we adjusted several parameters relating to driving tendencies under the same initial states.

Among the longitudinal control parameters in Table 1, T_h, α, ed, and λ relate very closely to the driver's lane changing tendencies. T_h and α determine the size of the desired safe spacing. As mentioned in Section IV (A.1), the desired spacing is proportional to T_h multiplied by the subject-vehicle velocity; however, it is inversely proportional to α multiplied by the relative velocity (e.g., if the subject- and lead-vehicles drive at 70 *km/h* and 80 *km/h*, respectively, the subject-vehicle requires approximately a 4.8m spacing when $T_h = 0.5$ and $\alpha = 0.1$, but a 2.9m spacing when $T_h = 0.4$ and $\alpha = 0.1$ and a 2.1m spacing when $T_h = 0.5$ and $\alpha = 0.15$). ed is another critical parameter that determines the size of the desired safe spacing in the LC mode execution. Adjusting this parameter can result in severe collisions in the LC mode, hence we left it unchanged. λ is used to calculate the magnitude of the desired acceleration, which ensures the desired spacing. Namely, we implemented various human-like controls such as cautious [Scenario (g)] and aggressive [Scenario (h)] driving by adjusting T_h, α, and λ; we set the values of these parameters to 0.6, 0.1, and 0.8 in Scenario (g), and 0.4, 0.2, and 1.2 in Scenario (h), respectively.

By comparing these simulation results, we can see that the LC mode was executed after lag-spacing control for LCSR in both scenarios, but it was initiated later in Scenario (g) (10.3 s) than in Scenario (h) (2.0 s). In Scenario (g), we determined that the ALCS was very tight [as shown in Figure 11(g)], and longitudinal acceleration chattering occurred due to repetitive lag-spacing, cruising, and lag-spacing controller switching, as shown in Figure 13(g). However, the magnitude of the chattered acceleration was small (within $\pm 0.5 m/s^2$); thus, the vehicle motion stability did not suffer any adverse impacts. However, we estimated that some influence was exerted on driver comfort and traffic flow.

In Scenario (h), we identified the subject-vehicle's motion to be more stable and smooth [Figure 13(h)]; however, the LC mode was executed even though the relative distance to the lag-vehicle was only secured at approximately 2 m [as shown in Figure 11(h)]. Thus, we estimate that a high-risk collision might occur with the lag-vehicle. Moreover, comparing the total energy of these scenarios, a lower value ($3.62 m/s^2$ lower) was measured in the aggressive driving setting [Scenario (h)], but vehicle safety was more strongly ensured in the cautious driving setting [Scenario (g)].

3) COLLISION RISK SITUATION-BASED EVALUATION

To assess whether our system avoids forward collisions, consistent decelerations were applied at $t = 0$ to the initial velocity of the lead- and front-vehicle in Scenario (i) ($-0.48 m/s^2$) and Scenario (j) ($-0.38 m/s^2$), respectively; for this, we used the same initial surrounding states, which required lag-spacing control. The surrounding conditions for front-vehicle deceleration in Scenario (l) matched those of Scenario (j); the results are discussed in the next section.

In Scenario (i), depending on the mode process (Table 2), the subject-vehicle initially performed lag-spacing control for LCSR; then, it executed minimal front-spacing controls for a short period (approximately 1.0 s). Meanwhile, the

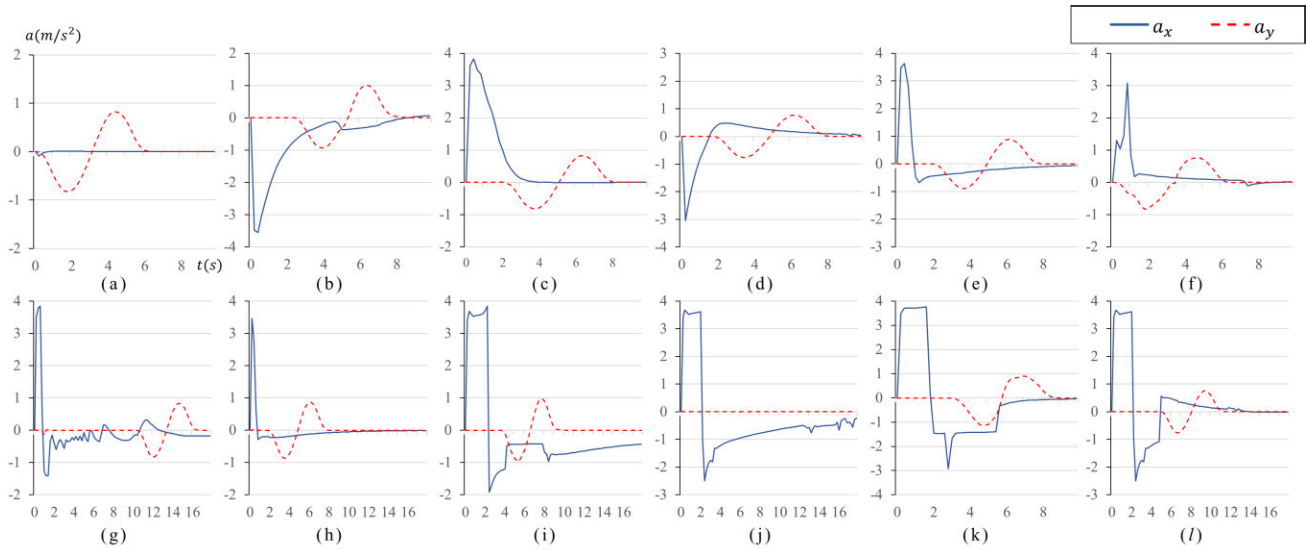

FIGURE 13. Longitudinal and lateral acceleration plots of subject vehicle for each scenario.

vehicle reached the LCS and implemented the LC mode (at 3.8 s). However, deceleration control was performed during the LC to ensure a safe distance with the decelerating lead-vehicle. Figure 11(i) shows that the desired distance to the lead-vehicle increased over time (until 3.8 s) prior to LC mode execution, owing to the deceleration of the lead-vehicle; then, it was decreased by the lead-spacing control in the LC mode. It is also shown in Figure 12(i) that—in accordance with Assumption 3 in Section III (B)—the lag-vehicle decelerated along with the decelerating forward vehicles. In addition, owing to the simultaneous control of the deceleration and steering during lane changes, the subject-vehicle had a slightly larger lateral acceleration (as shown in Table 3); however, the values were within $\pm 1 m/s^2$ and did not impede the stability of the vehicle.

The early phase of the subject-vehicle's movement in Scenario (j) was similar to that in Scenario (i), with some lag-spacing control observed. Subsequently, the subject-vehicle performed front-spacing control in the HDA mode under the influence of front-vehicle deceleration; thus, it failed to reach the LCS and maintained safe front-spacing control within the current lane [Figures 11 and 12 (j)]. In this case, to enhance the realism of the scenario, another ALCS search was required [addressed in Scenario (*l*)]; however, in this scenario, only the initially specified ALCS was maintained without change, following Assumption 1 in Section III (B). However, this scenario can occur in real driving situations, in which a ALCS cannot be selected because of the high-density flow in the target lane; thus, this result is significant and sufficiently descriptive.

4) ALCS SELECTION BASED EVALUATION

Our autonomous lane changing system is designed to perform decision-making and control separately, and it aims to control the vehicle such that it can reach the ALCS, regardless of where the ALCS—selected in the decision-making process—is situated. In this study, even though we specified a reasonable ALCS for control [following Assumption 1 in Section III (B)], Scenarios (d), (e), (k), and (*l*) allowed for system assessment according to ALCS selection.

Consider the situation shared between Scenarios (d) and (e) [i.e., there were three adjacent vehicles in target lane, these vehicles and the subject-vehicle drove at the same velocity, and the sizes of the selected ALCSs and distances to the subject-vehicle were identical. However, the ALCS was selected to the subject-vehicle's rear in Scenario (d) and to its front in Scenario (e)]; here, it is difficult to determine the nearest ALCS, but the situation is often encountered in real driving. As a result, controls to reach the LCS and change lanes were carried out smoothly in both scenarios. As shown in Figure 11(d) and (e), the LC mode was executed approximately at the same time in Scenario (d), but it can be seen that Scenario (d) (where the ALCS was selected slightly further back and deceleration was required for LCSR) was more energy efficient ($1.45 m/s^2$ lower) and general.

In Scenario (k), the ALCS was selected further ahead of the subject-vehicle. This selection can occur in situations where the empty adjacent spaces are very narrow and the distance to the front-vehicle is sufficiently safe. As a result, we verified that both LCS (through conducting lag- and lead-spacing control) and lane changing were performed successfully [as shown in Figure 11 (k)]. Notably, the subject-vehicle's movement was smoothly synchronized with the traffic flow, even though the velocity of the vehicle had increased through the acceleration required to reach the space [i.e., the velocities of the subject-vehicle and target-lane vehicles approached each other, as shown in Figure 12(k)]. In this respect, deceleration was inevitable; this caused a relatively large lateral acceleration ($-1.13 m/s^2$) during the LC mode but did not impede the stability of the vehicle motion.

In the aforementioned all scenarios, the specified ALCS was maintained during the simulation, and it can be assumed

that this setting sufficiently reflects a typical driver's behavior (i.e., the selected ALCS is set as a target and maintained continuously). In addition, excessively rapid changes to ALCS selection may impair system performance and result in unstable driving. However, in some situations, ALCS switching is required for effective driving. In this respect, the system assessment in Scenario (l) was also conducted in situations in which reasonable ALCS switching was required whilst driving.

In Scenario (l), we used a simple condition to switch the ALCS to an adjacent space (i.e., the lead- and lag-vehicles were interchanged) if the space was sufficiently empty whilst the subject-vehicle was not at the LCS. This scenario implemented the same conditions as Scenario (j). Scenario (j) showed that the subject-vehicle could not reach the LCS, because the continuously computed ALCS was inefficient; however, safe HDA was conducted, as previously addressed. In Scenario (l), the mode process results for the early phases of the subject-vehicle's movement were similar to those of Scenario (j) (i.e., some lag-spacing control and front-spacing control); however, after 3 s, the ALCS was switched [as shown in Figure 11(l)] and the vehicles used for control reference were re-selected (e.g., the lag-vehicle (before 3 s) became the lead-vehicle and the vehicle behind the lag-vehicle (before 3 s) became the lag-vehicle). After 3s, the new ALCS was selected and maintained until the simulation completed. At 2.4 seconds after the ALCS switch [Figures 12 and 13, Scenario (l)], we confirmed that controls to ensure a safe distance with the lead-vehicle were performed to reach the LCS. After LCSR, acceleration was applied through cruise control (in the LC mode), to maintain the speed at 70 *km/h*. With this, we verify the high security performance of our system in complex driving processes.

Furthermore, we validated the system for the case of a continuously varying ALCS selection. The results replicated those found for Scenario (j) (i.e., failure to perform lane change and repeated switching of HDA and LCSR modes). We omit these scenarios from this paper.

In all scenarios, in addition, the differences between the pre-designed LCO and controlled vehicle were observed to be less than 0.09 m (on average) during lane changes. In this respect, we verified that our system solves the existing dynamic instability problem caused by longitudinal acceleration variability in lateral control.

VI. CONCLUSION

This paper presented an autonomous lane change control system that is capable of adapting to variable surrounding conditions, thereby ensuring vehicle safety and traffic flow stability. We suggest a system architecture that consists of deep learning-based decision-making and dynamics model-based control procedures for optimal human-like ALCS selection and robust, autonomous lane change control. We designed a lane change procedure and focused on constructing a controller that could reach the ALCS and change the lanes robustly. For improved multi-motion and organic control with other ADASs already in use, a decoupled control structure and longitudinal trajectory-free control approach were suggested.

To validate the effectiveness of our system, simulated experiments were performed for 12 scenarios; these sufficiently considered situations that may arise in stable traffic flow. A system assessment was conducted based on four evaluation perspectives. As a result, we confirmed that our system ensures a high performance in both controlling the vehicle safely (i.e., with respect to the variable surrounding vehicles) and also ensuring the stability of vehicle motion. We also verified that our controller solves the existing dynamic instability problem caused by longitudinal acceleration variability in lateral control. Another significant advantage of this research is that the controlled vehicle does not interfere with the target-lane traffic flow and smoothly synchronizes with the flow during lane changing.

Future work will concentrate on expanding the deep learning-based ALCS-selection research, by training with more empirical lane changing data and expanding the results of this work therewith. More sophisticated parameters and gain tuning (through updating with state-of-the-art driver behavior analysis and reflecting the driving characteristics) will be performed. Hardware-in-the-loop simulations and actual vehicle-based tests will be conducted, and we plan to apply our system to vehicle-to-vehicle communication. In the future, we expect to tackle more complex autonomous lane changing situations (e.g., forced lane changing) using our system. 3.

REFERENCES

[1] J. D. Chovan, L. Tijerina, G. Alexander, and D. L. Hendricks, "Examination of lane change crashes and potential IVHS countermeasures," Nat. Highway Traffic Saf. Admin. U.S. Dept. Transp., Washington, DC, USA, Tech. Rep DOT HS 808 701, 1994.
[2] C. Bax, P. Leroy, and M. P. Hagenzieker, "Road safety knowledge and policy: A historical institutional analysis of The Netherlands," *Transp. Res. F: Traffic Psychol. Behav.*, vol. 25, pp. 127–136, Jul. 2014.
[3] J. S. Wang and R. R. Knipling, "Lane change/merge crashes: Problem size assessment and statistical description," Nat. Highway Traffic Saf. Admin. U.S. Dept. Transp., Washington, DC, USA, Tech. Rep DOT HS 808 075, 1994.
[4] C. Rodemerk, S. Habenicht, A. Weitzel, H. Winner, and T. Schmitt, "Development of a general criticality criterion for the risk estimation of driving situations and its application to a maneuver-based lane change assistance system," in *Proc. IEEE Intell. Vehicles Symp.*, Jun. 2012, pp. 264–269.
[5] D. Gonzalez, J. Perez, V. Milanes, and F. Nashashibi, "A review of motion planning techniques for automated vehicles," *IEEE Trans. Intell. Transp. Syst.*, vol. 17, no. 4, pp. 1135–1145, Apr. 2016.
[6] V. Butakov and P. Ioannou, "Personalized driver/vehicle lane change models for ADAS," *IEEE Trans. Veh. Technol.*, vol. 64, no. 10, pp. 4422–4431, Oct. 2015.
[7] L. Habel and M. Schreckenberg, "Asymmetric lane change rules for a microscopic highway traffic model," in *Cellular Automata*, vol. 8751. 2014, pp. 620–629.
[8] N. Lin, C. Zong, M. Tomizuka, P. Song, Z. Zhang, and G. Li, "An overview on study of identification of driver behavior characteristics for automotive control," *Math. Problems Eng.*, vol. 2014, Mar. 2014, Art. no. 569109.

[9] T. Toledo, O. Musicant, and T. Lotan, "In-vehicle data recorders for monitoring and feedback on drivers' behavior," *Transp. Res. C, Emerg. Technol.*, vol. 16, no. 3, pp. 320–331, 2008.
[10] Y. Lin, P. Tang, W. J. Zhang, and Q. Yu, "Artificial neural network modelling of driver handling behaviour in a driver-vehicle-environment system," *Int. J. Vehicle Des.*, vol. 37, no. 1, pp. 24–45, 2005.
[11] G. Xi and Y. Qun, "Driver—Vehicle—Environment closed—Loop simulation of handling and stability using fuzzy control theory," *Vehicle Syst. Dyn.*, vol. 23, no. 1, pp. 172–181, 1994.
[12] K. Santhanakrishnan and R. Rajamani, "On spacing policies for highway vehicle automation," in *Proc. Amer. Control Conf. (ACC)*, Chicago, IL, USA, Jun. 2000, pp. 1509–1513.
[13] R. Rajamani, H.-S. Tan, B. Kait Law, and W.-B. Zhang, "Demonstration of integrated longitudinal and lateral control for the operation of automated vehicles in platoons," *IEEE Trans. Control Syst. Technol.*, vol. 8, no. 4, pp. 695–708, Jul. 2000.
[14] G. Marsden, M. McDonald, and M. Brackstone, "Towards an understanding of adaptive cruise control," *Transp. Res. C, Emerg. Technol.*, vol. 9, no. 1, pp. 33–51, Feb. 2001.
[15] J. Wang and R. Rajamani, "The impact of adaptive cruise control systems on highway safety and traffic flow," *Proc. Inst. Mech. Eng., D, J. Automobile Eng.*, vol. 218, no. 2, pp. 111–130, 2004.
[16] J. Zhou and H. Peng, "Range policy of adaptive cruise control vehicles for improved flow stability and string stability," *IEEE Trans. Intell. Transp. Syst.*, vol. 6, no. 2, pp. 229–237, Jun. 2005.
[17] P. G. Gipps, "A model for the structure of lane-changing decisions," *Transp. Res. B, Methodol.*, vol. 20, no. 5, pp. 403–414, Oct. 1986.
[18] P. Hidas, "Modelling vehicle interactions in microscopic simulation of merging and weaving," *Transp. Res. C, Emerg. Technol.*, vol. 13, no. 1, pp. 37–62, 2005.
[19] J. A. Laval and C. F. Daganzo, "Lane-changing in traffic streams," *Transp. Res. B, Methodol.*, vol. 40, no. 3, pp. 251–264, Mar. 2006.
[20] T. Toledo, H. N. Koutsopoulos, and M. Ben-Akiva, "Integrated driving behavior modeling," *Transp. Res. C, Emerg. Technol.*, vol. 15, no. 2, pp. 96–112, Apr. 2007.
[21] J.-T. Kim, J. Kim, and M. Chang, "Lane-changing gap acceptance model for freeway merging in simulation," *Can. J. Civil Eng.*, vol. 35, no. 3, pp. 301–311, Mar. 2008.
[22] A. Kondyli, *Breakdown Probability Model at Freeway-Ramp Merges Based on Driver Behavior*. Belle Glade, FL, USA: Univ. Florida, 2009.
[23] W. Xiaorui and Y. Hongxu, "A lane change model with the consideration of car following behavior," *Procedia-Social Behav. Sci.*, vol. 96, pp. 2354–2361, Nov. 2013.
[24] Z. Zheng, S. Ahn, D. Chen, and J. Laval, "The effects of lane-changing on the immediate follower: Anticipation, relaxation, and change in driver characteristics," *Transp. Res. C, Emerg. Technol.*, vol. 26, pp. 367–379, Jan. 2013.
[25] Z. Guo, H. Wan, Y. Zhao, H. Wang, and Z. Li, "Driving simulation study on speed-change lanes of the multi-lane freeway interchange," *Procedia-Social Behav. Sci.*, vol. 96, pp. 60–69, Nov. 2013.
[26] Y. Hou, P. Edara, and C. Sun, "Situation assessment and decision making for lane change assistance using ensemble learning methods," *Expert Syst. Appl.*, vol. 42, no. 8, pp. 3875–3882, May 2015.
[27] N. Sledge and K. Marshek, "Comparison of ideal vehicle lane-change trajectories," *SAE Trans.*, vol. 106, no. 6, pp. 2004–2027, 1997.
[28] J. He, J. S. McCarley, and A. F. Kramer, "Lane keeping under cognitive load: Performance changes and mechanisms," *Hum. Factors: J. Hum. Factors Ergonom. Soc.*, vol. 56, no. 2, pp. 414–426, Mar. 2013.
[29] H. Yoshida, S. Shinohara, and M. Nagai, "Lane change steering manoeuvre using model predictive control theory," *Vehicle Syst. Dyn.*, vol. 46, no. sup1, pp. 669–681, Sep. 2008.
[30] P. Falcone, F. Borrelli, J. Asgari, H. E. Tseng, and D. Hrovat, "Predictive active steering control for autonomous vehicle systems," *IEEE Trans. Control Syst. Technol.*, vol. 15, no. 3, pp. 566–580, May 2007.
[31] P. Falcone, H. E. Tseng, F. Borrelli, J. Asgari, and D. Hrovat, "MPC-based yaw and lateral stabilisation via active front steering and braking," *Vehicle Syst. Dyn.*, vol. 46, no. 1, pp. 611–628, 2008.
[32] C. E. Beal and J. C. Gerdes, "Model predictive control for vehicle stabilization at the limits of handling," *IEEE Trans. Control Syst. Technol.*, vol. 21, no. 4, pp. 1258–1269, Jul. 2013.
[33] R. Zhang, Z. Zhang, Z. Guan, Y. Li, and Z. Li, "Autonomous lane changing control for intelligent vehicles," *Cluster Comput.*, vol. 22, no. S4, pp. 8657–8667, Jul. 2019.
[34] J. Funke, M. Brown, S. M. Erlien, and J. C. Gerdes, "Collision avoidance and stabilization for autonomous vehicles in emergency scenarios," *IEEE Trans. Control Syst. Technol.*, vol. 25, no. 4, pp. 1204–1216, Jul. 2017, doi: 10.1109/TCST.2016.2599783.
[35] S. Cheng, L. Li, H.-Q. Guo, Z.-G. Chen, and P. Song, "Longitudinal collision avoidance and lateral stability adaptive control system based on MPC of autonomous vehicles," *IEEE Trans. Intell. Transp. Syst.*, vol. 21, no. 6, pp. 2376–2385, Jun. 2020, doi: 10.1109/TITS.2019.2918176.
[36] J. Ji, A. Khajepour, W. W. Melek, and Y. Huang, "Path planning and tracking for vehicle collision avoidance based on model predictive control with multiconstraints," *IEEE Trans. Veh. Technol.*, vol. 66, no. 2, pp. 952–964, Feb. 2017.
[37] J. E. Naranjo, C. Gonzalez, R. Garcia, and T. de Pedro, "Lane-change fuzzy control in autonomous vehicles for the overtaking maneuver," *IEEE Trans. Intell. Transp. Syst.*, vol. 9, no. 3, pp. 438–450, Sep. 2008.
[38] H. Wang, B. Liu, X. Ping, and Q. An, "Path tracking control for autonomous vehicles based on an improved MPC," *IEEE Access*, vol. 7, pp. 161064–161073, 2019.
[39] B. Zhu, Y. Chen, J. Zhao, and Y. Su, "Design of an integrated vehicle chassis control system with driver behavior identification," *Math. Problems Eng.*, vol. 2015, Sep. 2015, Art. no. 954514.
[40] J. Nilsson, M. Brannstrom, E. Coelingh, and J. Fredriksson, "Lane change maneuvers for automated vehicles," *IEEE Trans. Intell. Transp. Syst.*, vol. 18, no. 5, pp. 1087–1096, May 2017, doi: 10.1109/TITS.2016.2597966.
[41] H. Zheng, J. Zhou, Q. Shao, and Y. Wang, "Investigation of a longitudinal and lateral lane-changing motion planning model for intelligent vehicles in dynamical driving environments," *IEEE Access*, vol. 7, pp. 44783–44802, 2019, doi: 10.1109/ACCESS.2019.2909273.
[42] B. Zhu, Z. Liu, J. Zhao, and W. Deng, "Driver behavior characteristics identification strategy for adaptive cruise control system with lane change assistance," SAE Tech. Paper 2017-0432, 2017, doi: 10.4271/2017-01-0432.
[43] R. Dang, J. Wang, S. E. Li, and K. Li, "Coordinated adaptive cruise control system with lane-change assistance," *IEEE Trans. Intell. Transp. Syst.*, vol. 16, no. 5, pp. 2373–2383, Oct. 2015, doi: 10.1109/TITS.2015.2389527.
[44] K. C. Dey, L. Yan, X. Wang, Y. Wang, H. Shen, M. Chowdhury, L. Yu, C. Qiu, and V. Soundararaj, "A review of communication, driver characteristics, and controls aspects of cooperative adaptive cruise control (CACC)," *IEEE Trans. Intell. Transp. Syst.*, vol. 17, no. 2, pp. 491–509, Feb. 2016, doi: 10.1109/TITS.2015.2483063.
[45] P. Wang, C.-Y. Chan, and A. de La Fortelle, "A reinforcement learning based approach for automated lane change maneuvers," in *Proc. IEEE Intell. Vehicles Symp. (IV)*, Changshu, China, Jun. 2018, pp. 1379–1384, doi: 10.1109/IVS.2018.8500556.
[46] S. Sharma, G. Tewolde, and J. Kwon, "Lateral and longitudinal motion control of autonomous vehicles using deep learning," in *Proc. IEEE Int. Conf. Electro Inf. Technol. (EIT)*, Brookings, SD, USA, May 2019, pp. 1–5, doi: 10.1109/EIT.2019.8833873.
[47] M. Arielle, "A model-free control algorithm derived using the sliding model control method," M.S. thesis, Rochester Inst. Technol., Rochester, NY, USA, 2015. [Online]. Available: https://scholarworks.rit.edu/theses/8666

JINSOO KIM received the B.S. and M.S. degrees in traffic engineering from Hanyang University, Seoul, South Korea, in 2010 and 2012, respectively, where he is currently pursuing the Ph.D. degree in mechanical convergence engineering and automotive engineering with the Graduate School. Since 2013, he has been a Research Assistant with the Institute of Mechanical Technology, Hanyang University. His research interests include the development of autonomous driving systems, intelligent traffic systems, and mobility as a service (MaaS) based on traffic flow and vehicle dynamics control and deep learning.

JAHNG-HYON PARK received the B.S. and M.S. degrees in mechanical engineering from Seoul National University, Seoul, South Korea, in 1983 and 1985, respectively, and the Ph.D. degree in mechanical engineering from the Massachusetts Institute of Technology, Cambridge, MA, USA, in 1992. He has been a Professor with Hanyang University, Seoul, since 1994. As a versatile and innovative scientist, his research activities have encompassed a wide spectrum of control engineering, sensor fusion system of a vehicle and robot, intelligent mobile robot systems, optimal control system of a 7-DOF hybrid robot arm, and an advanced driving assistance system (ADAS).

KYUNG-YOUNG JHANG received the B.S. and M.S. degrees in precision mechanical engineering from Hanyang University, Seoul, South Korea, in 1983 and 1985, respectively, and the Ph.D. degree in precision mechanical systems design from the Tokyo Institute of Technology, Yokohama, Japan, in 1991. He has been a Professor with Hanyang University, Seoul, since 1992. As a Visiting Professor, he worked with Johns Hopkins University, in 1999, and UC Irvine, in 2008. Recently, he has served as a Vice-President of KSNT in 2012. As a versatile and innovative scientist, his research activities encompass a wide spectrum of experimental mechanics, ultrasonic measurement, optical measurement, laser-material interactions, and advanced driving assistance system (ADAS).